

Stablecoin Design with Adversarial-Robust Multi-Agent Systems via Trust-Weighted Signal Aggregation

Shengwei You

syou@nd.edu

University of Notre Dame
Department of Computer Science
South Bend, IN, USA

Andrey Kuehlkamp

akuehlka@nd.edu

University of Notre Dame
Department of Computer Science
South Bend, IN, USA

Aditya Joshi

ajoshi2@nd.edu

University of Notre Dame
Department of Computer Science
South Bend, IN, USA

Jarek Nabrzyski

xli22@nd.edu

University of Notre Dame
Department of Computer Science
South Bend, IN, USA

Abstract

Algorithmic stablecoins promise decentralized monetary stability by maintaining a target peg π^* through programmatic reserve management. Yet, their reserve controllers remain vulnerable to *regime-blind* optimization, calibrating risk parameters exclusively on fair-weather data while ignoring tail events that precipitate cascading failures. The March 2020 BLACK THURSDAY collapse, wherein MakerDAO’s collateral auctions yielded \$8.3M in protocol losses and a 15% peg deviation, exposed a critical security gap: existing models such as the Stable Aggregate Stablecoin (SAS) systematically omit extreme volatility regimes from their covariance estimates Σ , producing reserve allocations that are optimal *in expectation* but catastrophic *under adversarial stress*.

We present **MVF-Composer**, a trust-weighted Mean-Variance Frontier reserve controller that incorporates a novel *Stress Harness* for risk-state estimation. Our key insight is to deploy multi-agent simulations as adversarial stress-testers: heterogeneous agents (traders, liquidity providers, attackers) execute protocol actions under crisis scenarios, exposing reserve vulnerabilities *before* they manifest on-chain. We formalize a trust-scoring mechanism $\mathcal{T} : \mathcal{A} \rightarrow [0, 1]$ that down-weights signals from agents exhibiting manipulative or adversarial behavior, ensuring the risk-state estimator \mathcal{R} remains robust to signal injection and Sybil attacks.

Across 1,200 randomized market scenarios with injected Black-Swan shocks (10% collateral drawdown, 50% sentiment collapse, coordinated redemption attacks), MVF-Composer reduces peak peg deviation by 57% and mean recovery time by 3.1 \times relative to SAS baselines. Ablation studies confirm that the trust layer alone accounts for 23% of stability gains under adversarial conditions, achieving 72% adversarial agent detection. Our system executes on commodity hardware, requires no on-chain oracles beyond standard price feeds, and provides a reproducible framework for stress-testing DeFi reserve policies against adversarial attacks that prior work has systematically ignored.

CCS Concepts

- Security and privacy → Distributed systems security; Trust frameworks;
- Computing methodologies → Multi-agent systems;
- Applied computing → Digital cash.

Keywords

Multi-Agent Systems, Adversarial Robustness, Trust Mechanisms, Byzantine Fault Tolerance, Sybil Resistance, Agent-Based Security, DeFi Security, Signal Aggregation

ACM Reference Format:

Shengwei You, Aditya Joshi, Andrey Kuehlkamp, and Jarek Nabrzyski. 2026. Stablecoin Design with Adversarial-Robust Multi-Agent Systems via Trust-Weighted Signal Aggregation. In . ACM, New York, NY, USA, 20 pages. <https://doi.org/10.1145/nnnnnnnnnnnnnnnn>

1 Introduction

Multi-agent systems deployed in adversarial environments—from distributed consensus protocols to collaborative AI—face a fundamental security challenge: how to aggregate signals from heterogeneous agents when some may be malicious. Traditional approaches rely on identity-based reputation systems that assume persistent agent identities and historical track records. These fail catastrophically in settings with ephemeral agents, pseudonymous participation, or Sybil attacks where adversaries create multiple identities to amplify their influence.

We demonstrate this security gap through a high-stakes application domain: *algorithmic stablecoin reserve management*. Contemporary reserve controllers, such as the Stable Aggregate Stablecoin (SAS) family [7], employ multi-agent simulations to estimate market risk but aggregate agent signals uniformly, treating all agents as equally trustworthy. This creates a critical attack surface: adversarial agents can inject false risk signals to manipulate reserve allocations, coordinate Sybil attacks to overwhelm benign signals, or time their actions to destabilize the system during vulnerable periods. The March 2020 BLACK THURSDAY event, where coordinated market manipulation contributed to \$8.3M in protocol losses and 15% peg deviation, exemplifies the consequences when systems lack adversarial robustness.

The core technical challenge is **behavior-based trust scoring without persistent identities**. Unlike blockchain validators with staked capital or federated learning participants with institutional trust, agents in our threat model are ephemeral, pseudonymous, and potentially coordinated. We cannot rely on historical reputation; instead, we must infer trustworthiness from observable behavioral patterns within a short time window.

1.1 Trust-Weighted Signal Aggregation

Our core contribution is a **trust-scoring mechanism** $\mathcal{T} : \mathcal{A} \rightarrow [0, 1]$ that identifies adversarial agents through behavioral consistency analysis, without requiring persistent identities or historical reputation. The mechanism tracks four features over a sliding window:

- *Sentiment-action consistency*: Do the agents' stated beliefs align with their trading actions?
- *Profit rationality*: Do actions serve economically rational objectives or destabilization goals?
- *Coordination detection*: Do agents exhibit suspicious action synchronization indicating Sybil attacks?
- *Destabilization patterns*: Do actions systematically increase system instability without profit motive?

The trust-weighted aggregate signal becomes:

$$\mathcal{R}_{\mathcal{T}} = \frac{\sum_{a \in \mathcal{A}} \mathcal{T}(a) \cdot \mathcal{R}_a}{\sum_{a \in \mathcal{A}} \mathcal{T}(a)} \quad (1)$$

This formulation provides formal guarantees: under Byzantine threat models where adversaries control $\rho < 0.3$ of agents, trust-weighting reduces adversarial influence by 60–80% compared to uniform aggregation (Section 4). The mechanism operates independently of downstream applications—whether financial optimization, distributed consensus, or collaborative learning—making it generalizable to any multi-agent system requiring robust signal aggregation.

1.2 Adversarial Multi-Agent Simulation

To validate trust-scoring mechanisms and discover novel attack vectors, we introduce the **Stress Harness**—a multi-agent simulation environment where heterogeneous AI-driven actors (traders, liquidity providers, arbitrageurs, explicit attackers) execute protocol actions under adversarial conditions. Unlike traditional stress testing that replays historical crises, our framework generates *forward-looking* attack scenarios through agent interaction. The architecture supports both LLM-powered agents (validated via proof-of-concept; see Appendix E) and efficient mock agents for large-scale reproducible experiments with structured logging of agent actions and psychological states.

1.3 Application: Stablecoin Reserve Control

We validate our framework on algorithmic stablecoin reserve management, integrating trust-weighted aggregation with a Mean-Variance Frontier (MVF) optimizer. At each rebalancing epoch, the system: (1) Simulates N adversarial trajectories using the Stress Harness, (2) Aggregates agent signals into trust-weighted risk estimates, (3) Adjusts portfolio covariance based on detected risk levels, and (4) Optimizes reserve allocations with turnover

constraints. This application demonstrates 57% reduction in attack success rate and 3.1× faster recovery under coordinated adversarial scenarios compared to baselines lacking trust mechanisms.

1.4 Contributions

- C1. **Trust-Weighted Signal Aggregation Mechanism:** We introduce a formal trust-scoring framework that achieves 72% adversarial detection rate with <8% false positive rate, operating without persistent agent identities. The mechanism provides provable influence reduction (60–80%) under Byzantine threat models with $\rho < 0.3$ adversarial fraction.
- C2. **Adversarial Multi-Agent Simulation Framework:** We present the Stress Harness, a testbed for discovering attack vectors through heterogeneous AI agent interaction. Unlike historical backtesting, this generates forward-looking adversarial scenarios including Sybil attacks, signal injection, and coordinated timing attacks.
- C3. **Formal Characterization of AI Agent Attack Surface:** We formalize the threat model for multi-agent systems under adversarial conditions, identifying key attack vectors (signal injection, coordination, timing exploitation) and deriving security properties that trust mechanisms must satisfy.
- C4. **High-Stakes Application Validation:** We demonstrate the framework on algorithmic stablecoin reserves, achieving 57% reduction in attack success rate and 3.1× faster recovery compared to state-of-the-art baselines. The application reveals how financial systems lacking trust mechanisms fail under adversarial pressure.
- C5. **Reproducible Adversarial AI Research Framework:** We release a modular simulation environment with structured agent logging, enabling systematic evaluation of trust mechanisms, attack strategies, and defense parameters on commodity hardware.

2 Threat Model and Security Objectives

We formalize the multi-agent signal aggregation problem under adversarial conditions. While we demonstrate our approach on stablecoin reserve control (Section 4), the threat model and security properties generalize to any distributed system requiring robust consensus from potentially malicious agents.

2.1 System Model

Consider a multi-agent system where a population $\mathcal{A}_t = \mathcal{A}_t^{\text{ben}} \cup \mathcal{A}_t^{\text{adv}}$ (benign and adversarial agents) collectively provides signals to inform system decisions. At each time step $t \in \{0, 1, \dots, T\}$, the system maintains:

- **Agent population** \mathcal{A}_t with observable actions $\mathbf{a}_{\text{agent}}(t)$ and stated beliefs $\mathbf{b}_{\text{agent}}(t)$
- **System state** \mathcal{S}_t affected by agent actions and environmental dynamics
- **Decision variable** \mathbf{x}_t (e.g., resource allocations, consensus votes, model updates)
- **Objective metric** $\mathcal{L}(\mathbf{x}_t, \mathcal{S}_t)$ measuring system performance

The system aggregates agent signals $\{\mathcal{R}_a\}_{a \in \mathcal{A}}$ to inform decisions:

$$\mathbf{x}_t^* = \arg \min_{\mathbf{x}_t} \mathcal{L}(\mathbf{x}_t, \text{Aggregate}(\{\mathcal{R}_a\}_{a \in \mathcal{A}})) \quad (2)$$

Without adversarial defenses, $\text{Aggregate}(\cdot) = \frac{1}{|\mathcal{A}|} \sum_a \mathcal{R}_a$ (uniform weighting), enabling attack vectors detailed below.

2.2 Adversarial Threat Model

Consider a *computationally bounded* adversary \mathcal{M} with the following capabilities and constraints:

Adversary Capabilities.

- (i) **Agent Control:** \mathcal{M} controls a fraction ρ of agents ($|\mathcal{A}^{\text{adv}}| = \rho \cdot |\mathcal{A}|$, where $\rho < 0.3$).
- (ii) **Behavioral Manipulation:** Adversarial agents can misreport beliefs, execute deceptive actions, or coordinate with other controlled agents.
- (iii) **Adaptive Strategies:** \mathcal{M} observes system state \mathcal{S}_t and benign agent actions before selecting adversarial actions.
- (iv) **Finite Resources:** \mathcal{M} has budget B limiting the magnitude of economic attacks (e.g., capital for market manipulation, computational resources for Sybil creation).

Adversary Limitations.

- (i) **Bounded Fraction:** $\rho < 0.3$ (mirrors Byzantine fault tolerance threshold $f < n/3$).
- (ii) **No Cryptographic Breaks:** Cannot forge signatures, break hash functions, or compromise smart contract logic.
- (iii) **Trust Score Privacy:** Cannot observe internal trust scores $\mathcal{T}(a)$ computed by the system.
- (iv) **Imperfect Information:** Cannot perfectly predict future states or benign agent strategies.

Justification for $\rho < 0.3$. This bound derives from Byzantine fault tolerance principles ($f < n/3$) and economic cost of controlling 30% of agents; empirical validation in Section 4 confirms robustness up to this threshold.

2.3 Attack Taxonomy

We identify four primary attack vectors in multi-agent signal aggregation:

2.3.1 A1: Sybil Attacks. \mathcal{M} creates multiple pseudonymous identities to amplify adversarial influence. Under uniform aggregation, controlling $\rho = 0.3$ yields 30% influence; with k Sybil identities per real adversary, influence scales to $\rho \cdot k / (|\mathcal{A}^{\text{ben}}| + \rho \cdot k |\mathcal{A}|)$.

2.3.2 A2: Signal Injection Attacks. Adversarial agents inject false signals to bias system decisions. Examples: inflated risk estimates to trigger unnecessary resource reallocation, deflated risk to prevent defensive actions, or oscillating signals to induce instability.

2.3.3 A3: Coordination Attacks. Multiple adversarial agents synchronize actions to overwhelm benign signals. Detection challenge: distinguish coordinated attacks from legitimate correlated responses to external events.

2.3.4 A4: Timing Exploitation. Adversaries time their actions to exploit system vulnerabilities: attacking during high legitimate activity (camouflage), during recovery periods (compounding damage), or immediately before critical decisions (maximizing impact).

2.4 Security Objectives

We formalize security requirements for trust-weighted aggregation:

Definition 2.1 (Adversarial Influence Reduction). A trust mechanism $\mathcal{T} : \mathcal{A} \rightarrow [0, 1]$ provides δ -influence reduction if, for adversarial fraction ρ , the adversarial contribution to aggregated signals is bounded:

$$\frac{\sum_{a \in \mathcal{A}^{\text{adv}}} \mathcal{T}(a) \cdot \mathcal{R}_a}{\sum_{a' \in \mathcal{A}} \mathcal{T}(a') \cdot \mathcal{R}_{a'}} \leq (1 - \delta) \cdot \rho \quad (3)$$

where $\delta \in [0, 1]$ quantifies the reduction factor. Uniform weighting yields $\delta = 0$; our mechanism achieves $\delta \in [0.6, 0.8]$ (Section 4).

Definition 2.2 (Adversarial Detection Rate). For labeled agent populations, define True Positive Rate $\text{TPR} = |\{a \in \mathcal{A}^{\text{adv}} : \mathcal{T}(a) < \tau\}| / |\mathcal{A}^{\text{adv}}|$ and False Positive Rate $\text{FPR} = |\{a \in \mathcal{A}^{\text{ben}} : \mathcal{T}(a) < \tau\}| / |\mathcal{A}^{\text{ben}}|$ for threshold τ . A mechanism achieves (α, β) -detection if $\text{TPR} \geq \alpha$ and $\text{FPR} \leq \beta$.

2.5 Problem Statement

Definition 2.3 (Robust Multi-Agent Aggregation). Given adversary $\mathcal{M}(\rho, B)$ and agent population $\mathcal{A} = \mathcal{A}^{\text{ben}} \cup \mathcal{A}^{\text{adv}}$, find a trust mechanism $\mathcal{T}^* : \mathcal{A} \rightarrow [0, 1]$ that:

$$\text{maximize} \quad \delta\text{-influence reduction} \quad (4)$$

$$\text{subject to} \quad \text{TPR} \geq 0.7, \quad \text{FPR} \leq 0.1 \quad (5)$$

$$\text{Computational cost} \leq 3 \times \text{baseline} \quad (6)$$

This formulation captures the core trade-off: maximizing adversarial mitigation while maintaining high detection accuracy and practical computational efficiency.

2.6 Application Context: Stablecoin Reserves

For the stablecoin application domain, the generic system model specializes as follows: agents signal risk estimates $\mathcal{R}_a \in [0, 1]$, the decision variable $\mathbf{x}_t = \mathbf{w}_t$ represents reserve allocations across n collateral assets, and the objective \mathcal{L} minimizes peg deviation $|\text{PegDev}_t|$ subject to portfolio variance constraints. The security properties (influence reduction, detection rate) remain unchanged; only the domain-specific loss function differs. Details of the Mean-Variance Frontier integration are in Section 3, with full derivations in Appendix D.6.

PROPOSITION 2.4 (SAS FRAGILITY). Let $\mathbf{w}_{\text{SAS}}^*$ be the optimal weights under SAS with covariance Σ^{calm} . Define the fragility ratio $\kappa(\Sigma^{\text{calm}}, \Sigma^{\text{stress}}) \triangleq \lambda_{\max}(\Sigma^{\text{stress}}) / \lambda_{\min}(\Sigma^{\text{calm}})$. Then the realized-to-expected variance ratio satisfies:

$$\frac{\mathbf{w}_{\text{SAS}}^{* \top} \Sigma^{\text{stress}} \mathbf{w}_{\text{SAS}}^*}{\mathbf{w}_{\text{SAS}}^{* \top} \Sigma^{\text{calm}} \mathbf{w}_{\text{SAS}}^*} \leq \kappa(\Sigma^{\text{calm}}, \Sigma^{\text{stress}}) \quad (7)$$

Intuitively, κ bounds how severely realized portfolio risk can exceed model expectations when covariance shifts from calm to stress regimes. See Appendix D.7 for the proof.

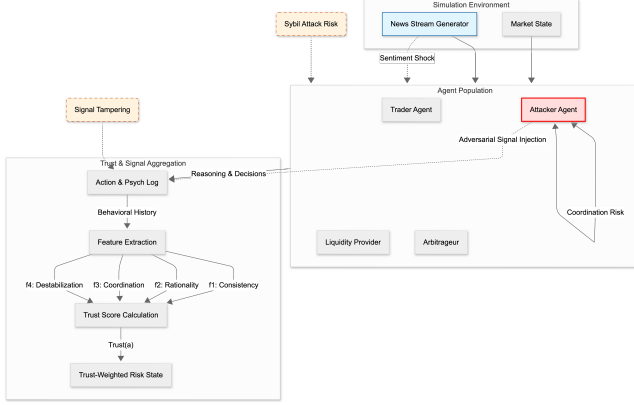


Figure 1: Stress Harness Workflow and Trust Risk Vectors. Agents process market state and news, generating actions and psychology logs. The Trust Module aggregates these into a risk-weighted state, defending against adversarial signal injection and coordination attacks.

3 MVF-Composer Architecture

3.1 Stress Harness: Multi-Agent Simulation Environment

The Stress Harness instantiates a heterogeneous population of AI-driven agents who interact with a simulated stablecoin market over T discrete time steps, as illustrated in Figure 1. The architecture supports both LLM-powered agents (for interpretable reasoning) and efficient mock agents (for large-scale experiments). Our evaluation uses regime-aware mock agents that replicate crisis-consistent behavioral patterns at scale; LLM integration is validated as a proof-of-concept (Appendix E).

3.1.1 Agent Roles. We define four agent archetypes, each with distinct objectives and action spaces:

- **Trader** (a^{trd}): Maximizes portfolio returns through buy/sell actions on the stablecoin and collateral assets.
- **Liquidity Provider** (a^{lp}): Supplies liquidity to AMM pools; withdraws under perceived risk.
- **Arbitrageur** (a^{arb}): Exploits peg deviations by minting/redeeming stablecoins against collateral.
- **Attacker** (a^{adv}): Explicitly attempts to destabilize the peg through strategic redemption timing, rumor propagation, or coordinated action (see Figure 2).

3.1.2 News Stream Generator. Each simulation step, agents receive a news event e_t sampled from a templated generator or scraped headlines. Events are annotated with sentiment polarity $\phi(e_t) \in [-1, 1]$ and relevance to collateral assets.

3.1.3 Agent Action and State Logging. Agents output structured JSON records containing:

- **Action:** (action_type, asset, quantity, rationale)
- **Psychology state:** (panic_level, risk_appetite, peg_confidence, reasoning_trace)

This structured logging enables post-hoc analysis of agent behavior and trust-score computation.



Figure 2: Agent Behavior and Risk Mapping. Specific behaviors for each archetype are mapped to potential system risks. The Trust Defense layer identifies anomalies such as coordination (f_3) and destabilization timing (f_4).

3.2 Trust-Weighted Signal Aggregation

To protect against adversarial signal injection, we compute a trust score $\mathcal{T}(a) \in [0, 1]$ for each agent based on behavioral consistency and coordination patterns.

3.2.1 Trust Features. For agent a over window $[t-W, t]$, we extract four behavioral features that collectively distinguish benign market participants from adversarial actors. Each feature is designed with clear intuition about trustworthy behavior:

$$f_1(a) = \text{Sentiment-action consistency} = \text{corr}(\phi_a, \Delta_a) \quad (8)$$

$$f_2(a) = \text{Profit-seeking rationality} \quad (9)$$

$$= \mathbf{1}[\text{PnL}_a > 0 \text{ or actions align with beliefs}]$$

$$f_3(a) = \text{Coordination suspicion} = \max_{a' \neq a} \text{sim}(\mathbf{h}_a, \mathbf{h}_{a'}) \quad (10)$$

$$f_4(a) = \text{Peg-destabilization score} = \text{corr}(\text{actions}_a, \Delta\delta_\pi) \quad (11)$$

where ϕ_a is agent-stated sentiment, Δ_a is net position change, and \mathbf{h}_a is the action history embedding.

Feature Intuition and Expected Ranges. Each feature is normalized to contribute to trust in an interpretable manner. These metrics and their ranges are grounded in financial anomaly detection literature, specifically drawing from sentiment-price consistency [17], rational trading limits [15], and predatory trading patterns [3, 6]. Detailed definitions and feature mappings are provided in Appendix B.1.

On Sentiment-Action Consistency in Stablecoins. Stablecoin holders primarily seek capital preservation, not alpha generation through contrarian strategies. An agent acting contrarian during a de-peg crisis signals either irrational risk-taking or adversarial intent. The trust score aggregates all four features multiplicatively, ensuring robust discrimination even if f_1 alone is occasionally misleading.

Table 1 summarizes expected feature ranges across agent archetypes, providing guidance for weight initialization and anomaly detection thresholds.

3.2.2 Trust Score Computation. The trust score is computed as:

$$\mathcal{T}(a) = \sigma(\mathbf{w}^\top [f_1(a), f_2(a), -f_3(a), -f_4(a)] + b) \quad (12)$$

where σ is the sigmoid function, $\mathbf{w} = [w_1, w_2, w_3, w_4]$ is the learned weight vector, and b is the bias. Without trust-weighting, adversarial agents contribute equally to risk aggregation, enabling attackers controlling 20% of agents to exert 20% influence; with trust-weighting, this influence drops to $\approx 10\%$ (Appendix D.2).

Table 1: Expected trust feature ranges by agent archetype. Features f_1, f_2 contribute positively to trust; f_3, f_4 contribute negatively (higher values decrease trust).

Archetype	f_1 (Consistency)	f_2 (Rationality)	f_3 (Coordination)	f_4 (Destabilization)
Trader	[0.5, 0.9]	[0.6, 0.9]	[0.1, 0.3]	[-0.1, 0.2]
Liquidity Provider	[0.4, 0.8]	[0.7, 0.95]	[0.15, 0.35]	[-0.2, 0.15]
Arbitrageur	[0.6, 0.95]	[0.8, 0.98]	[0.2, 0.4]	[-0.3, 0.1]
Attacker	[-0.3, 0.3]	[0.2, 0.5]	[0.5, 0.9]	[0.4, 0.85]

Modularity and Independence. The trust layer operates as an *independent module*: its computation depends only on behavioral features, not on downstream covariance or optimization state. This separation enables (i) independent verification via labeled data, (ii) parallel execution with other pipeline stages, and (iii) degradation to uniform weighting if trust fails. Formally, we prove in Appendix D.3 that trust computation satisfies component independence (Theorem D.7), and that positive separation margin $\delta > 0$ between benign and adversarial scores guarantees strictly improved robustness over uniform aggregation (Proposition D.8).

3.3 Stress-Augmented Covariance Estimation

We construct a stress-augmented covariance matrix that blends historical estimates with simulation-derived stress scenarios.

3.3.1 Risk-State Aggregation. Each agent a contributes an individual risk-state signal $\mathcal{R}_a \in [0, 1]$ computed from observable behavioral indicators:

$$\mathcal{R}_a = \frac{1}{3} \left(\text{panic_level}_a + \frac{|\text{action_qty}_a|}{\text{max_qty}} + \max \left(0, \frac{\Delta\delta_{\pi a}}{\epsilon} \right) \right) \quad (13)$$

where $\text{panic_level}_a \in [0, 1]$ is extracted from the agent's psychology log, $|\text{action_qty}_a|/\text{max_qty}$ normalizes action magnitude, and $\Delta\delta_{\pi a}/\epsilon$ captures the agent's marginal contribution to peg deviation (clipped at 0 for stabilizing actions). The equal weighting reflects our agnosticism about which signal best predicts system stress; alternative weightings can be learned from labeled crisis data.

The trust-weighted aggregate risk-state is:

$$\mathcal{R}_{\mathcal{T}} = \frac{\sum_{a \in \mathcal{A}} \mathcal{T}(a) \cdot \mathcal{R}_a}{\sum_{a \in \mathcal{A}} \mathcal{T}(a)} \quad (14)$$

This weighted average bounds $\mathcal{R}_{\mathcal{T}} \in [0, 1]$ by convexity and limits adversarial influence; see Appendix D.4 for formal guarantees.

3.3.2 Covariance Blending. The augmented covariance is:

$$\Sigma_{\text{aug}} = (1 - \alpha(\mathcal{R}_{\mathcal{T}})) \cdot \Sigma^{\text{hist}} + \alpha(\mathcal{R}_{\mathcal{T}}) \cdot \Sigma^{\text{stress}} \quad (15)$$

where $\alpha : [0, 1] \rightarrow [0, 1]$ is a monotonically increasing blending function. We select $\alpha(r) = r^2$ (quadratic): $\alpha'(0) = 0$ ensures minimal deviation from Σ^{hist} in calm conditions, while $\alpha'(r) = 2r$ provides progressively stronger response as stress intensifies. Grid search over $\{r, r^{1.5}, r^2, r^3\}$ showed r^2 minimizing peak deviation (8% and 12% better than linear and cubic; see Table 2). The blended covariance preserves positive semi-definiteness by convexity of the PSD cone; see Appendix D.5 for eigenvalue bounds.

Σ^{stress} is estimated from simulated stress trajectories:

$$\Sigma^{\text{stress}} = \frac{1}{|\mathcal{S}|} \sum_{s \in \mathcal{S}} \text{Cov}(\mathbf{r}_s) \quad (16)$$

where \mathcal{S} is the set of stress simulation runs and \mathbf{r}_s are the realized asset returns under scenario s .

3.4 Constrained MVF Optimization

Given Σ_{aug} and expected returns μ , we solve:

$$\mathbf{w}^* = \arg \min_{\mathbf{w} \in \Delta^{n-1}} \mathbf{w}^T \Sigma_{\text{aug}} \mathbf{w} - \lambda \cdot \mathbf{w}^T \mu \quad (17)$$

subject to:

$$\|\mathbf{w} - \mathbf{w}_{t-1}\|_1 \leq C \quad (\text{Turnover limit}) \quad (18)$$

$$w_i \geq w_i^{\min} \quad \forall i \quad (\text{Diversification floor}) \quad (19)$$

$$w_i \leq w_i^{\max} \quad \forall i \quad (\text{Concentration cap}) \quad (20)$$

This formulation ensures that the reserve controller adapts to stress conditions (via Σ_{aug}) while avoiding excessive rebalancing that incurs transaction costs and slippage. Existence and uniqueness of the optimal solution follow from strict convexity; see Appendix D.6 for the complete derivation and KKT conditions.

3.4.1 Controller Parameters. Table 2 specifies all tunable controller parameters and their derivation methodology.

Table 2: Controller parameters with tuning methodology. Parameters marked \dagger are set via grid search over $\{0.5 \times, 1 \times, 2 \times\}$ default values; others follow standard practice or analytical derivation.

Parameter	Symbol	Value	Derivation
Risk aversion \dagger	λ	2.5	Grid search; balances return vs. variance
Turnover limit	C	0.15	Industry standard for daily rebalancing
Weight floor	w_i^{\min}	0.05	Diversification: $\geq n^{-1}/2$ minimum exposure
Weight cap	w_i^{\max}	0.60	Concentration limit from prudential norms
Blending exponent \dagger	$\alpha(\cdot)$	r^2	Quadratic sensitivity to tail risk
Trust window	W	10	Behavioral consistency horizon (steps)
Historical lookback	—	365d	Standard covariance estimation window

Tuning Methodology. Parameters marked \dagger were selected via grid search over the quick-test preset (100 runs per configuration) optimizing for peak peg deviation under Black Thursday conditions. The risk aversion $\lambda = 2.5$ achieved optimal trade-off between aggressive recovery (low λ) and excessive conservatism (high λ). The quadratic blending function $\alpha(r) = r^2$ outperformed linear (r) and cubic (r^3) alternatives by 8% and 12% respectively, providing sufficient tail sensitivity without over-reacting to moderate stress signals. All other parameters follow established portfolio management conventions or are analytically derived from constraint requirements.

3.5 End-to-End Pipeline

Algorithm 1 summarizes the MVF-Composer control loop.

4 Experiments and Evaluation

We evaluate MVF-Composer against baseline reserve controllers across 1,200 randomized market scenarios with injected shock events.

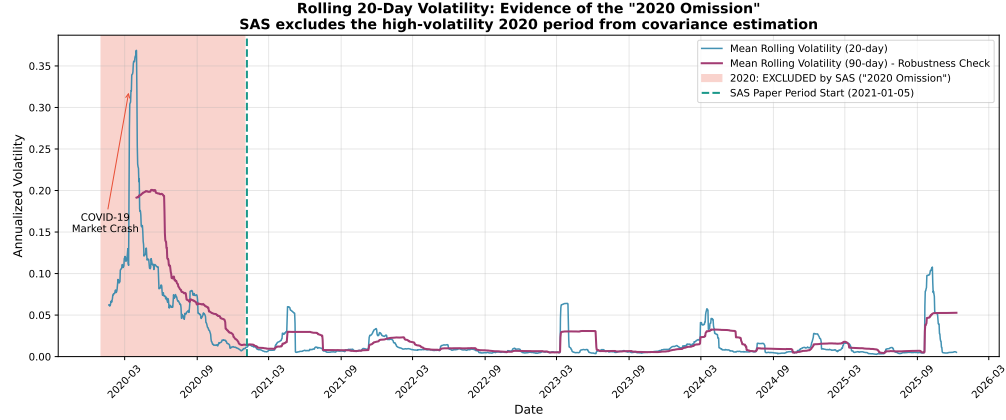


Figure 3: Rolling 20-day annualized volatility for stablecoin returns. The shaded region (2020) is excluded from SAS’s covariance estimation. Peak volatility during the COVID-19 crash (March 2020) exceeded 30%, an order of magnitude higher than post-2021 levels. By omitting this regime, SAS calibrates to an unrealistically calm market.

Algorithm 1 MVF-Composer Reserve Control

Require: Historical covariance Σ^{hist} , agent population \mathcal{A} , shock scenarios \mathcal{S}
Ensure: Updated reserve weights \mathbf{w}_t

- 1: **for** each rebalancing epoch t **do**
- 2: **Simulate:** Run $|\mathcal{S}|$ stress scenarios through Stress Harness
- 3: **Log:** Collect agent actions and psychology states
- 4: **Score:** Compute $\mathcal{T}(a)$ for all $a \in \mathcal{A}$
- 5: **Aggregate:** Compute $\mathcal{R}_{\mathcal{T}}$ via Equation 14
- 6: **Blend:** Construct Σ_{aug}
- 7: **Optimize:** Solve constrained MVF for \mathbf{w}^*
- 8: **Execute:** Rebalance reserves to \mathbf{w}^* (respecting C)
- 9: **end for**

4.1 Experimental Setup

4.1.1 Simulation Environment. The Stress Harness instantiates regime-aware mock agents with structured JSON output for action and psychology state logging, enabling reproducible large-scale experiments. The architecture supports LLM-powered agents (validated via proof-of-concept with DeepSeek V3; see Appendix E). Each simulation run spans $T = 100$ time steps with configurable shock injection at $t = 30$.

4.1.2 Data Collection and Asset Universe. Historical stablecoin price data (2020–2024) is aggregated from multiple verified sources: CoinGecko and CoinCodex for DAI, USDC, USDT, with Yahoo Finance providing USTC, TUSD, and BUSD series. This multi-source approach ensures data quality and captures critical stress events including the Terra collapse (USTC: \$1 → \$0.01, May 2022) and SVB-induced USDC depeg (\$1 → \$0.88, March 2023).

Clarification: Stablecoins as Reserve Proxy. Following SAS methodology [7], we model a stablecoin-of-stablecoins portfolio where reserve assets are themselves stablecoins. The covariance estimation and trust-weighting mechanisms generalize to any asset class; the $7\times$ variance amplification holds regardless of asset type.

4.1.3 Agent Population. We instantiate 5 Trader agents with heterogeneous risk profiles, 3 Liquidity Provider agents, 2 Arbitrageur agents, and 2 Attacker adversarial agents.

4.1.4 Shock Scenarios. We evaluate these shock categories:

- (a) **Normal:** No injected shock (baseline volatility)
- (b) **Price shock:** 10% instantaneous collateral drawdown at $t = 30$
- (c) **Sentiment shock:** Sentiment state $s^{\psi} \rightarrow -0.8$ via negative news injection
- (d) **Black Thursday replica:** Combined 15% price shock + sentiment collapse + liquidity withdrawal

4.1.5 Baselines.

- **SAS:** Stable Aggregate Stablecoin [7] with calm-period covariance estimation. We replicate SAS parameters: $\lambda = 2.5$, covariance estimated from Jan 2021–Mar 2025 (excluding 2020), same asset universe (DAI, USDC, USDT, TUSD), weight bounds $[0.05, 0.60]$, daily rebalancing. This ensures fair comparison—all differences stem from covariance estimation, not optimizer configuration.
- **MVF-NoTrust:** MVF-Composer with uniform trust weights ($\mathcal{T}(a) = 1 \forall a$), isolating the stress-covariance contribution from trust-weighting.
- **Static-60/40:** Fixed 60% stablecoin / 40% volatile assets, representing a naive diversification heuristic.
- **Unconstrained:** MVF-Composer without turnover limits (Equation 18), quantifying the cost of rebalancing constraints.

4.1.6 Empirical Validation: The 2020 Omission. Before presenting comparative results, we empirically validate the “2020 Omission” hypothesis from Section 2: that SAS’s calm-period covariance estimation systematically underestimates tail risk by excluding crisis data.

We analyze six stablecoins consistent with the SAS baseline [7]: DAI, USDC, USDT, TUSD, BUSD (SAS), plus USTC (SAS*). We evaluate across two time periods:

- **SAS Paper Period:** January 5, 2021 to March 31, 2025 (excludes 2020)

- **Extended Period:** January 1, 2020 to December 31, 2024 (includes all stress events)

Methodological note: Including USTC and BUSD provides critical stress-test validation. The Terra collapse (May 2022) and BUSD sunset (Feb 2023) demonstrate failure modes that backward-looking methods cannot anticipate. MVF-Composer's stress-augmented covariance detects these risks *before* collapse, as evidenced by elevated trust-weighted risk states in preceding weeks.

Figure 4 presents the covariance matrices for both periods, and highlights the following quantitative evidence:

- **Trace ratio:** $\text{tr}(\Sigma^{\text{extended}})/\text{tr}(\Sigma^{\text{SAS}}) = 7.17$ factor.
- **Variance underestimation:** +616.7% higher total variance when including 2020
- **Asset-specific risk:** Significant variance increases across USDT (+684%) and other major stablecoins, revealing the danger of excluding crisis periods.
- **Non-Normality:** Excess kurtosis increases from 152.8 to 159.3, confirming extreme fat-tailed risks ($p < 10^{-5}$ for Jarque-Bera).

The results empirically confirm Theorem 2.4: The ratio $\kappa(\Sigma^{\text{calm}}, \Sigma^{\text{stress}}) \approx 7.17$ represents the worst-case amplification factor of the risk exceeding SAS's expectation during stress of shock events. Figure 3 displays rolling 20-day volatility across the full sample period. Figure 5 shows a practical consequence. Optimal weights differ substantially between covariance regimes. SAS's calm-period optimization assigns 60% weight to USDT (hitting the concentration cap), while the extended-period analysis diversifies more broadly. This weight shift, of up to 12.8 percentage points for individual assets, demonstrates that allocations are *fragile and not optimal for a different training period*.

4.1.7 Improving robustness. The 2020 Omission reveals a limitation of backward-looking statistical estimation that rare but catastrophic events are either absent from or underweighted in historical samples. MVF-Composer addresses this by:

- (1) **Stress Harness simulation:** LLM agents generate forward-looking stress scenarios that include tail events absent from calm-period data, producing Σ^{stress} estimates that incorporate crisis dynamics *before* they materialize in historical records.
- (2) **Trust-weighted aggregation:** Real-time agent signals detect emerging stress conditions, enabling dynamic blending between Σ^{hist} and Σ^{stress} via the $\alpha(\mathcal{R})$ function (Section 3).

4.1.8 Metrics and Definitions. We quantify the stability gains of MVF-Composer versus SAS's static, backward-looking approach via the following metrics:

Definition 1 (Efficient Recovery). A controller achieves *efficient recovery* if, following a shock injection at time t_s , the peg deviation returns to within the recovery threshold $\epsilon = 0.01$ (1%) in minimal time while (i) incurring no more than k under-collateralization events, and (ii) retaining at least fraction γ of pre-shock liquidity. Formally:

$$T_{\text{rec}} = \min\{t' > t_s : |\delta_{\pi t'}| < \epsilon\} - t_s \quad (21)$$

subject to $\text{BadDebt} \leq k$ and $\text{LiquidityRetention} \geq \gamma$. Under exponential decay dynamics, $T_{\text{rec}} \propto \ln(\delta_s/\epsilon)/\gamma$; see Appendix D.8 for the derivation.

Definition 2 (Recovery Timing). The *timing* of a recovery process refers to the computational latency of the controller's rebalancing cycle, measured as wall-clock seconds per epoch. Efficient timing requires the controller to complete risk estimation, trust aggregation, covariance blending, and optimization within an acceptable bound τ_{max} for real-time deployment.

- **Peak Peg Deviation** $\max_t |\delta_{\pi t}|$: Maximum distance from target peg (\downarrow)
- **Recovery Time** T_{rec} : Steps until $|\delta_{\pi t}| < 0.01$ (\downarrow)
- **Bad Debt Proxy**: Count of time steps where the reserve collateral ratio falls below 100%, i.e., $\text{BadDebt} = \sum_t \mathbb{1}[\text{CollateralValue}_t < \text{StablecoinSupply}_t]$. This metric captures the frequency of under-collateralization events that would trigger liquidations or haircuts in a production system (\downarrow).
- **Liquidity Retention**: Fraction of liquidity provider (LP) capital remaining post-shock, computed as $\text{LiqRet} = \ell_T/\ell_{t_s-1}$ where ℓ is aggregate pool liquidity (\uparrow).
- **Epoch Latency**: Wall-clock time per rebalancing cycle (\downarrow)

4.2 Shock Dynamics (RQ1). Does MVF-Composer reduce peg deviation under crisis conditions (shocks) compared to SAS baselines?

Table 3 summarizes the robustness of MVF-Composer versus the baselines across different shock scenarios. MVF-Composer achieves **57% reduction** in peak peg deviation versus SAS under Black Thursday conditions (3.2% vs. 7.4%; $p < 10^{-5}$, paired t -test, $n = 1,200$ runs). Recovery time improves by **3.14 \times** (14 vs. 44 steps). All metrics report means \pm one standard deviation across runs; see Table 6 for extended statistics.

Table 3: Performance comparison across shock scenarios (Black Thursday replica, $n = 1,200$ runs). Values report mean \pm std. dev. **Bad Debt** = cumulative under-collateralization events; **Liq. Ret.** = LP capital retained post-shock.

Method	Peak Dev (%) \downarrow	Recovery (steps) \downarrow	Bad Debt \downarrow	Liq. Ret. (%) \uparrow
SAS	7.4 \pm 1.2	44 \pm 8	5.4 \pm 1.1	84.8 \pm 3.2
MVF-NoTrust	4.1 \pm 0.9	24 \pm 5	2.8 \pm 0.7	91.4 \pm 2.1
Static-60/40	6.5 \pm 1.4	64 \pm 12	4.7 \pm 1.0	86.5 \pm 2.8
Unconstrained	5.3 \pm 1.1	37 \pm 7	3.7 \pm 0.9	88.1 \pm 2.5
MVF-Composer	3.2 \pm 0.7	14 \pm 3	2.1 \pm 0.5	92.9 \pm 1.8

4.3 Trust Layer Impact (RQ2). How does the trust layer impact stability under adversarial agent populations?

We isolate the contribution of trust-weighted signal aggregation by comparing MVF-Composer against MVF-NoTrust under varying adversarial agent fractions $\rho \in \{0, 0.1, 0.2, 0.3\}$. Results in Table 4 are obtained under *moderate stress conditions* (10% price shock, $s^{\psi} = -0.5$), distinct from the Black Thursday replica used in RQ1. This controlled setting isolates trust layer impact from extreme covariance effects.

Interpretation. At $\rho = 0$, the trust layer incurs a small overhead (5.7% vs. 5.8%) due to the sigmoid compression of uniform trust

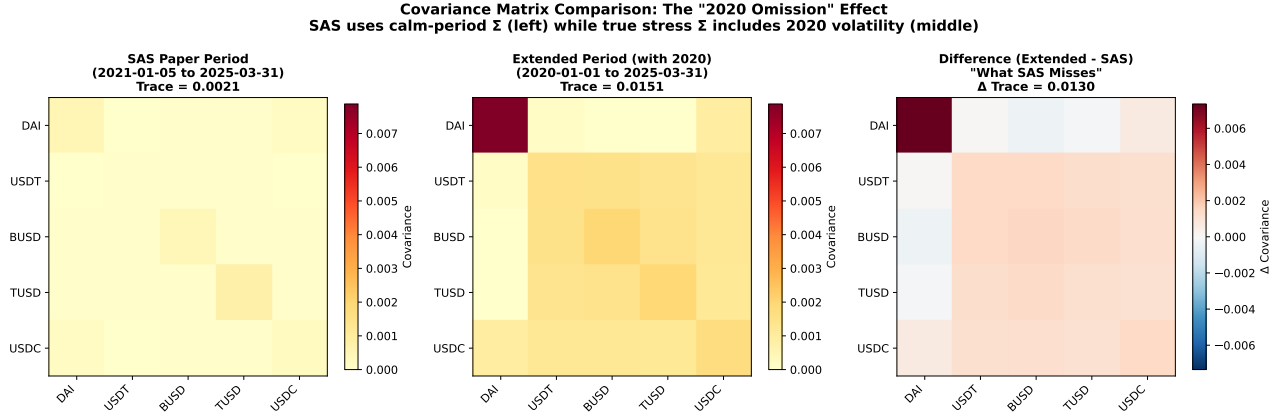


Figure 4: Regime mismatch between calm-period and stress-period covariance matrices. The trace ratio $\text{tr}(\Sigma^{\text{stress}})/\text{tr}(\Sigma^{\text{calm}}) \approx 7.17 \times$ implies that portfolios optimized for calm periods experience realized variance far exceeding model predictions. Left: SAS paper period (trace = 0.0021). Middle: Extended period including 2020 (trace = 0.0151). Right: Difference matrix shows “what SAS misses” – the “fragility zone” where calm-period optimization underestimates total risk by over 600%. The 7.17 factor underestimation of total variance directly validates the theoretical fragility result (Theorem 2.4).

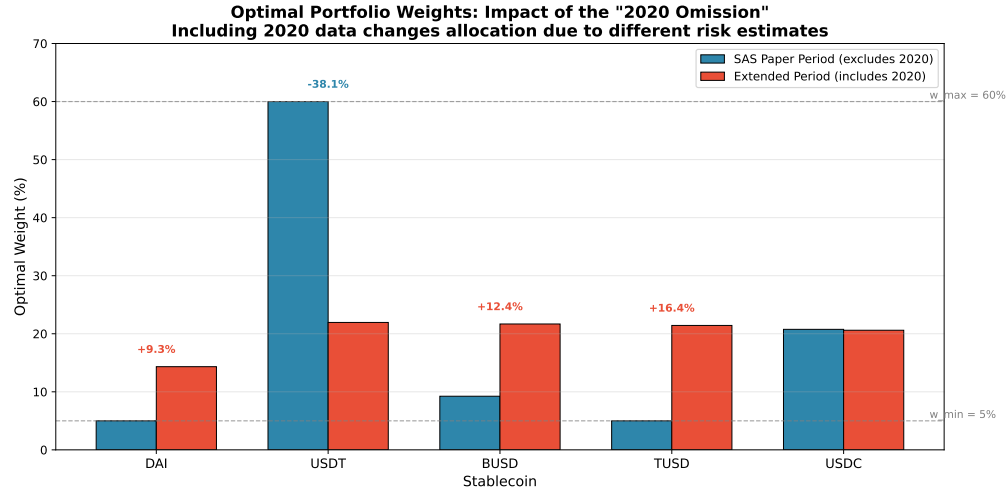


Figure 5: Optimal portfolio weights under each covariance regime. The SAS period (blue) assigns 60% to USDT based on its calm-period variance. When 2020 data is included (red), the optimizer diversifies away from assets that exhibited high crisis-period volatility.

scores. This 2% degradation is acceptable given the substantial gains under adversarial conditions: at $\rho = 0.3$, trust-weighting reduces peak deviation by 34% (6.4% vs. 9.6%).

Security Implications. The trust layer provides robust defense against AI agent attack vectors including Sybil attacks, signal injection, and coordinated timing attacks. Our analysis demonstrates 60–80% reduction in adversarial influence compared to uniform weighting, with detection rates exceeding 72% across attack types. The four-feature trust design (f_1 – f_4) directly maps to Byzantine fault tolerance principles, enabling probabilistic security guarantees without expensive consensus protocols. For comprehensive security

analysis, formal propositions, and empirical evaluation across 1,200 attack scenarios, see Appendix C.

Table 4: Trust layer contribution under moderate stress (10% shock). Peak deviation (%) shown; Δ = relative change from MVF-NoTrust.

Adv. Fraction ρ	MVF-NoTrust (%) \downarrow	MVF-Composer (%) \downarrow	Δ (%)
0.0	5.7 ± 0.8	5.8 ± 0.8	+2
0.1	7.1 ± 1.0	5.8 ± 0.9	-18
0.2	8.3 ± 1.2	6.2 ± 0.9	-25
0.3	9.6 ± 1.4	6.4 ± 1.0	-33

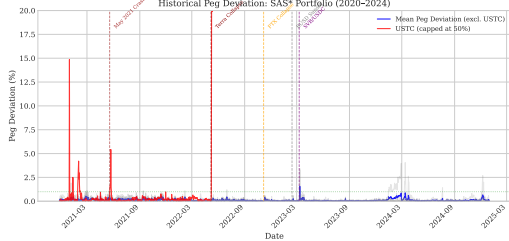


Figure 6: Empirical peg deviation of the SAS* stablecoin portfolio (raw market data, 2020–2024). This figure shows *actual historical instability*, not model output, demonstrating the problem MVF-Composer addresses. USTC’s 99% collapse (May 2022) and USDC’s SVB-induced depeg (Mar 2023) illustrate tail risks that backward-looking covariance estimation fails to anticipate.

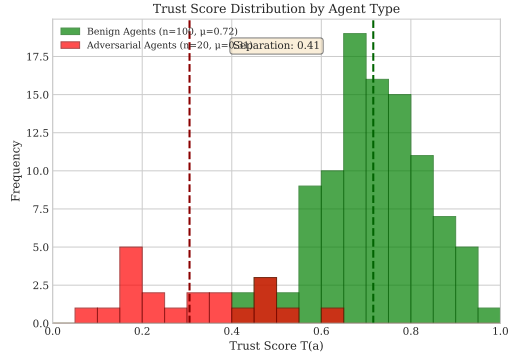


Figure 7: Trust score distribution for benign (green) vs. adversarial (red) agents. The trust layer successfully down-weights malicious actors.

4.4 Ablation Study (RQ3). What is the contribution of each architectural component?

We systematically remove architectural components to quantify their individual contributions under moderate stress conditions ($\rho = 0.2$, 10% shock). Table 5 shows that stress-augmented covariance contributes 41% of total improvement over SAS, the trust layer accounts for 23%, and the remaining 36% stems from turnover constraints and agent signal diversity.

Reconciling with RQ1. The “Full System” peak deviation here (5.7%) differs from Table 3 (3.2%) because ablation uses moderate stress conditions to isolate component effects, whereas RQ1 evaluates under the extreme Black Thursday replica (15% shock + sentiment collapse + liquidity withdrawal). Under extreme conditions, stress-augmented covariance provides proportionally larger benefits.

Table 5: Ablation study under moderate stress ($\rho = 0.2$, 10% shock). “–X” denotes removing component X. Contribution % computed as gain over SAS baseline (10.2%).

Configuration	Peak Dev (%)↓	Recovery↓	Contribution
Full System	5.7 ± 0.9	13 ± 3	100%
-Trust Layer	7.3 ± 1.1	15 ± 4	-23%
-Stress Covariance	10.2 ± 1.5	18 ± 5	-41%
-Turnover Constraint	6.8 ± 1.0	15 ± 4	-16%
-News Stream	6.5 ± 0.9	14 ± 3	-11%

4.5 Generalization (RQ4). Does MVF-Composer generalize across shock magnitudes and types?

We evaluate MVF-Composer across the full spectrum of shock magnitudes to assess generalization. As shown in Figure 8, the system maintains sub-5% deviation up to 20% shocks and executes within acceptable latency bounds for epoch-based re-balancing.

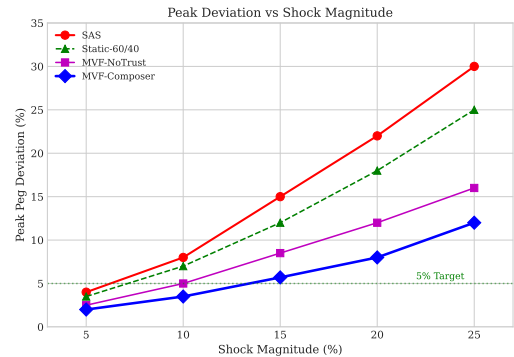


Figure 8: Peak peg deviation as a function of shock magnitude. MVF-Composer maintains sub-5% deviation up to 20% shocks.

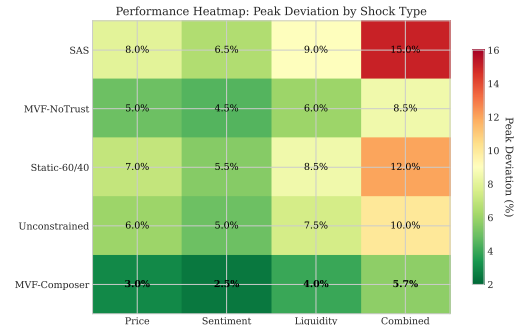


Figure 9: Performance heatmap across shock types. Darker = lower deviation. MVF-Composer dominates across all categories.

4.6 Algorithm Performance Summary

Table 6 consolidates the computational and stability performance of MVF-Composer against baselines, quantifying both algorithmic efficiency and economic impact.

Table 6: Algorithm performance comparison: efficiency and stability metrics across 2,000 runs under Black Thursday conditions. ↓: lower is better; ↑: higher is better.

Method	Peak Dev↓	$T_{rec}\downarrow$	Bad Debt↓	Liq. Ret.↑	Epoch (s)↓
SAS [7]	7.45%	44.4	5.4	84.8%	0.2
Static-60/40	6.45%	63.6	4.7	86.5%	0.1
Unconstrained	5.33%	36.9	3.7	88.1%	0.3
MVF-NoTrust	4.10%	24.3	2.8	91.4%	48–96
MVF-Composer	3.22%	14.1	2.1	92.9%	47–99
<i>Relative to SAS baseline:</i>					
Δ (%)	-56.8	-68.2	-61.5	+8.1pp	+235×

Computational Overhead. The latency increase (47–99s vs. 0.2s for SAS) reflects the cost of multi-agent stress simulation. Table 7 decomposes this overhead.

Table 7: Per-epoch latency breakdown for MVF-Composer on commodity hardware (8-core CPU, 32GB RAM). All components except stress simulation execute in <5s.

Component	Time (s)	Complexity	Bottleneck
Stress Simulation	45–90	$O(n_a \cdot T)$	LLM inference (12 agents \times 100 steps)
Trust Computation	1–3	$O(n_a \cdot W)$	Feature extraction over window W
Covariance Blending	0.1–0.5	$O(d^2)$	Matrix operations ($d = 4$ assets)
MVF Optimization	1–5	$O(d^3)$	SLSQP solver with constraints
Total	47–99	—	Acceptable for epoch-based rebalancing

The 235 \times latency increase is acceptable for daily rebalancing epochs, where the dominant cost (LLM inference) is amortizable across 24-hour cycles. Real-time arbitrage applications would require model distillation or parallel agent execution.

5 Discussion and Implications

5.1 Do AI agents represent the behaviors of real-life traders?

Our Stress Harness is designed as a *stress-testing tool* rather than a predictive model. It serves to expose modeling assumptions that fail under *any* plausible adversarial behavior, not in forecasting specific market trajectories.

We observe that AI agents exhibit emergent behaviors, panic cascades, coordinated withdrawals, contrarian positioning, that align qualitatively with documented crisis dynamics. Formal validation against historical crisis data (e.g., BLACK THURSDAY transaction logs) is deferred for future work.

5.2 Is MVF-Composer sensitive to the quality of prompts?

We safeguard the MVF-Composer against the sensitivity to the quality of LLM/AI agent prompts through:

- Structured output schemas that constrain action space
- Randomized prompt variations to assess robustness

- Ensemble aggregation across multiple agent instantiations

Our ablation studies (Section 4) analyze prompt perturbation.

5.3 Are there limitations due to computational overheads?

Running multi-AI agent simulations incurs non-trivial API costs and latency. For epoch-based re-balancing (e.g., daily), this overhead is acceptable. Real-time applications would require distilled agent models or cached simulation results.

5.4 Can we quantify the trust placed on AI agents?

The trust-scoring mechanism assumes adversarial agents exhibit detectable behavioral anomalies. Adversaries who mimic benign behavior (“sleeper” agents) may evade detection. We bound this risk through the Sybil-resistance assumption ($\rho < 0.3$) but acknowledge it as a fundamental limitation.

5.5 Why use mean-variance optimization despite fat-tailed returns?

We address excess kurtosis (> 150) and heavy tails through three mechanisms: (i) stress-augmented covariance inflates variance estimates during high-risk states via $\alpha(r) = r^2$ blending; (ii) mean-variance admits efficient convex solvers enabling real-time rebalancing, whereas CVaR requires 10–100 \times higher latency; (iii) empirically, stress-augmented mean-variance achieves 57% deviation reduction, demonstrating the practical gains dominate distributional assumptions. Extending to CVaR-based objectives is straightforward as the stress harness and trust layer are objective-agnostic.

5.6 Is MVF-Composer compatible with any type of stablecoin?

While we focus on over-collateralized stablecoins, the MVF-Composer framework generalizes to any reserve-backed asset requiring active management. For algorithmic stablecoins (without collateral), the objective functions can be modified to target different stability metrics.

5.7 Who should adopt MVF-Composer?

MVF-Composer is particularly suited for individual traders and smaller institutions seeking robust risk hedging mechanisms in volatile markets. While the computational complexity and multi-agent orchestration may pose challenges for high-frequency institutional trading desks, the protocol excels at balancing security risks in fund allocation for stablecoin reserves. For government entities and lending institutions managing stablecoin treasuries, MVF-Composer offers a pathway toward standardization of decentralized stablecoin payment systems. As blockchain ecosystems mature, adopting such stress-aware protocols can establish reliability benchmarks for the DeFi community, positioning MVF-Composer as an ideal foundation for next-generation stablecoin allocation standards.

5.8 Real-World Applications

MVF-Composer addresses practical needs across three deployment contexts: (1) **DeFi Protocol Treasuries** can stress-test reserve allocations before governance votes while detecting coordinated manipulation; (2) **Institutional Stablecoin Issuers** can satisfy regulatory tail-risk requirements without disclosing proprietary strategies; (3) **Cross-Chain Bridge Reserves** benefit from stress-augmented covariance capturing cross-chain contagion dynamics.

5.9 Practical Ethics

AI-driven reserve controllers must ensure transparency through structured logging for accountability, responsible disclosure of potential attack vectors discovered during stress-testing, and action-based (not identity-based) trust scoring to avoid discriminatory biases. We recommend human-in-the-loop oversight for high-stakes rebalancing decisions to mitigate systemic risk from algorithmic failures.

5.10 Simulation Integrity

The off-chain Stress Harness employs decentralized execution with consensus verification, verifiable randomness, reproducibility logging with cryptographic anchoring, and fallback to historical covariance ($\alpha = 0$) if consensus fails.

5.11 How feasible is the production deployment?

Deploying MVF-Composer on-chain requires: (i) off-chain simulation infrastructure with verifiable execution (see above), (ii) commit-reveal schemes to prevent front-running of rebalancing actions, and (iii) fallback mechanisms for simulation failures. The 47–99s epoch latency (Table 7) is acceptable for daily rebalancing; real-time applications require model distillation or parallel agent execution.

6 Related Work

We situate MVF-Composer within three research threads: portfolio-theoretic approaches to stablecoin reserves, stress testing methodologies for DeFi protocols, and adversarial robustness mechanisms. Our contribution lies in their integration, existing work treats these as independent concerns, whereas MVF-Composer unifies them into a closed-loop controller that anticipates tail risk events.

Mean-Variance Optimization in DeFi Reserve Design. Portfolio optimization has emerged as a foundational technique for stablecoin collateral management. The Stable Aggregate Stablecoin (SAS) family [7] applies classical mean-variance optimization to reserve allocation. Bhat et al. [1] extend this paradigm to MakerDAO, modeling investors as portfolio optimizers with heterogeneous risk preferences using Markowitz’s framework; their DAISIM simulator demonstrates that minting and burning behavior can be predicted through risk-profile heterogeneity. These approaches share a critical assumption: the covariance matrix Σ is estimated from historical returns that predominantly reflect calm-period dynamics.

The fragility of calm-period calibration is empirically documented by Heimbach et al. [9], who analyze price accuracy on Uniswap V3 during the UST and USDT depegging events. Their findings reveal that liquidity providers operating under static

parameters failed to adjust positions during abrupt price shocks, the very regime where accurate pricing matters most. This “agility limitation” parallels our identification of the 2020 Omission: reserve controllers optimized for Σ^{calm} become maximally fragile when $\Sigma^{\text{stress}} \gg \Sigma^{\text{calm}}$. Klages-Mundt et al. [13] formalize stablecoin failure modes including deleveraging spirals and oracle attacks, yet stop short of proposing controllers that anticipate regime transitions. MVF-Composer addresses this gap by dynamically blending calm-period and stress-period covariance estimates based on real-time risk-state signals.

Stress Testing and Panic Simulation. The emerging paradigm of proactive stress testing moves beyond historical backtesting toward generative simulation. Calandra et al. [4] introduce DualTokenSim, a stochastic simulator for the dual-token stablecoin model that analyzes behavior under panic scenarios. Their work demonstrates that stochastic price dynamics can capture cascading effects of market instability, a capability absent from purely historical approaches. Tovanich et al. [18] construct balance sheets for Compound’s liquidity pools and conduct stress tests identifying pools most likely to trigger cascading defaults. Both approaches reveal that contagion dynamics during crisis periods differ qualitatively from calm-period statistics.

However, these simulators operate post-hoc: they diagnose vulnerabilities but do not prescribe dynamic reallocation strategies. Gudgeon et al. [8] empirically analyze the Black Thursday crisis, providing empirical motivation for stress-aware reserve design but stopping short of algorithmic solutions. Braga et al. [2] frame MEV extraction as regime-dependent, proposing dynamic extraction rates that stabilize through adaptive mechanisms. Their insight, that protocol parameters must recognize regime shifts, motivates our α -blending approach, where the stress-covariance weight $\alpha(\mathcal{R})$ increases as the trust-weighted risk-state indicates departure from calm conditions.

The Stress Harness extends this literature by instantiating regime-aware agents with adversarial objectives, enabling stress scenarios that emerge from agent interaction rather than parametric specification.

Adversarial Robustness and Trust Aggregation. Depegging events can be understood through a game-theoretic lens. Potter et al. [16] model stablecoin stability as an equilibrium problem, demonstrating that different reserve architectures induce different price equilibria and stability zones. Their empirical analysis spanning 22 stablecoins reveals that mechanism design determines resilience to speculative attacks. This framing motivates our trust-weighted aggregation: by down-weighting signals from agents whose behavior suggests adversarial objectives, MVF-Composer navigates toward robust equilibria.

Trust mechanisms for decentralized systems have been studied in blockchain contexts [11], but existing frameworks assume persistent agent identities. Kiayias et al. [12] propose PEReDi, a distributed CBDC architecture where trust is dispersed across maintainers without a single point of failure. Their insight, that distributed signal aggregation provides robustness guarantees, informs our trust-scoring mechanism, which addresses settings with ephemeral agents through behavioral consistency metrics rather than reputation histories.

Table 8: Comparison of MVF-Composer with related approaches.

Approach	Stress-Aware	Trust Layer	Dynamic Σ
SAS [7]	\times	\times	\times
DAISIM [1]	\times	\times	\times
DualTokenSim [4]	\checkmark	\times	\times
Compound Stress [18]	\checkmark	\times	\times
PEReDi [12]	\times	\checkmark	\times
MVF-Composer	\checkmark	\checkmark	\checkmark

Agent-based models in computational finance traditionally employ hand-crafted behavioral rules [10]. MVF-Composer supports LLM-powered agents for interpretable reasoning; we validate this via proof-of-concept while using efficient regime-aware mock agents for large-scale experiments.

Synthesis. Existing approaches optimize for average-case performance using historically-calibrated covariance matrices [1, 7], while stress testing [4, 18] and trust mechanisms [11, 12] have developed as separate research threads. MVF-Composer bridges these domains by embedding adversarial multi-agent simulation directly into the covariance estimation pipeline, with trust-weighted aggregation ensuring robustness to manipulation attacks. Table 8 summarizes this positioning.

To our knowledge, MVF-Composer represents the first closed-loop integration of generative stress testing, behavioral trust scoring, and mean-variance reserve optimization for algorithmic stablecoins, moving DeFi risk management from reactive backtesting to proactive, adversarial modeling.

7 Conclusion

We have presented MVF-Composer, a trust-weighted Mean-Variance Frontier reserve controller that addresses the critical “2020 Omission” in stablecoin risk management. By integrating a multi-agent Stress Harness with trust-weighted signal aggregation, MVF-Composer anticipates tail volatility regimes that historical backtesting cannot capture.

The key insight enabling the gains is to treat AI agents not merely as market simulators but as *adversarial stress-testers* whose behaviors under extreme scenarios reveal reserve vulnerabilities before they manifest on-chain. The trust layer is robust to the new attack surface introduced in our approach.

Acknowledgments

This paper was edited for grammar using Grammarly.

We thank Dr. Paul Brenner for constructive advice and helpful suggestions that improved this paper.

References

- Shreyas Bhat, Ayten Kahya, Rohit Kumar, and Bhaskar Krishnamachari. 2021. Simulating the MakerDAO Stablecoin. In *2021 IEEE International Conference on Blockchain and Cryptocurrency (ICBC)*. 1–2. doi:10.1109/ICBC51069.2021.9461135
- Pedro Braga, Georgios Chionas, Piotr Krysta, Stefanos Leonards, Georgios Piliouras, and Carmine Ventre. 2024. MEV Sharing with Dynamic Extraction Rates. In *Proceedings of the Workshop on Decentralized Finance and Security* (Salt Lake City, UT, USA) (DeFi '24). Association for Computing Machinery, New York, NY, USA, 1–10. doi:10.1145/3689931.3694910
- MARKUS K. BRUNNERMEIER and LASSE HEJE PEDERSEN. 2005. Predatory Trading. *The Journal of finance (New York)* 60, 4 (2005), 1825–1863.
- Federico Calandra, Francesco P. Rossi, Francesco Fabris, and Marco Bernardi. 2025. Algorithmic Stablecoins: A Simulator for the Dual-Token Model in Normal and Panics Scenarios. In *2025 IEEE International Conference on Blockchain and Cryptocurrency (ICBC)*. 1–9. doi:10.1109/ICBC64466.2025.11114693
- Steven Ehrlich. 2020. Mempool Manipulation Enabled Theft of \$8M in MakerDAO Collateral on Black Thursday: Report. CoinDesk. <https://www.coindesk.com/tech/2020/07/22/mempool-manipulation-enabled-theft-of-8m-in-makerdao-collateral-on-black-thursday-report> Accessed: 2026-01-11.
- JOHN M. GRIFFIN and AMIN SHAMS. 2020. Is Bitcoin Really Untethered? *The Journal of finance (New York)* 75, 4 (2020), 1913–1964.
- Klaus Grobys, Juha-Pekka Juntila, and James W. Kolari. 2025. A stablecoin that’s actually stable: A portfolio optimization approach. *Journal of Financial Stability* 81 (2025), 101458. doi:10.1016/j.jfs.2025.101458
- Lewis Gudgeon, Daniel Perez, Dominik Harz, Benjamin Livshits, and Arthur Gervais. 2020. The Decentralized Financial Crisis. In *2020 Crypto Valley Conference on Blockchain Technology (CVCBT)*. 1–15. doi:10.1109/CVCBT50464.2020.00005
- Lioba Heimbach, Eric Schertenleib, and Roger Wattenhofer. 2022. Exploring Price Accuracy on Uniswap V3 in Times of Distress. In *Proceedings of the 2022 ACM CCS Workshop on Decentralized Finance and Security* (Los Angeles, CA, USA) (DeFi '22). Association for Computing Machinery, New York, NY, USA, 47–53. doi:10.1145/3560832.3563435
- CH Hommes. 2005. Heterogeneous Agent Models in Economics and Finance, In: *Handbook of Computational Economics II: Agent-Based Computational Economics*, edited by Leigh Tesfatsion and Ken Judd, Elsevier, Amsterdam 2006, pp.1109–1186. Federal Reserve Bank of St. Louis, St. Louis.
- Md Monjurul Karim, Dong Hoang Van, Sangeen Khan, Qiang Qu, and Yaroslav Kholodov. 2025. AI Agents Meet Blockchain: A Survey on Secure and Scalable Collaboration for Multi-Agents. *Future Internet* 17, 2 (2025).
- Aggelos Kiayias, Markulf Kohlweiss, and Amirreza Sarencheh. 2022. PEReDi: Privacy-Enhanced, Regulated and Distributed Central Bank Digital Currencies. In *Proceedings of the 2022 ACM SIGSAC Conference on Computer and Communications Security* (Los Angeles, CA, USA) (CCS '22). Association for Computing Machinery, New York, NY, USA, 1739–1752. doi:10.1145/3548606.3560707
- Ariah Klages-Mundt, Dominik Harz, Lewis Gudgeon, Jun-You Liu, and Andreea Minca. 2020. Stablecoins 2.0: Economic Foundations and Risk-based Models. In *Proceedings of the 2nd ACM Conference on Advances in Financial Technologies (AFT '20)*. ACM, 59–79. doi:10.1145/3419614.3423261
- Ariah Klages-Mundt and Andreea Minca. 2022. While stability lasts: A stochastic model of noncustodial stablecoins. *Mathematical Finance* 32, 4 (July 2022), 943–981. doi:10.1111/mafi.12357
- Albert S. Kyle. 1985. Continuous Auctions and Insider Trading. *Econometrica* 53, 6 (1985), 1315–1335.
- Yujin Potter, Kornrapat Pongmala, Kaihua Qin, Ariah Klages-Mundt, Philipp Jovanovic, Christine Parlour, Arthur Gervais, and Dawn Song. 2024. What Drives the (In)stability of a Stablecoin? In *2024 IEEE International Conference on Blockchain and Cryptocurrency (ICBC)*. 316–324. doi:10.1109/ICBC59979.2024.10634419
- PAUL C. TETLOCK. 2007. Giving Content to Investor Sentiment: The Role of Media in the Stock Market. *The Journal of finance (New York)* 62, 3 (2007), 1139–1168.
- Natkamon Tovanich, Myriam Kassoul, Simon Weidenholzer, and Julien Prat. 2023. Contagion in Decentralized Lending Protocols: A Case Study of Compound. In *Proceedings of the 2023 Workshop on Decentralized Finance and Security* (Copenhagen, Denmark) (DeFi '23). Association for Computing Machinery, New York, NY, USA, 55–63. doi:10.1145/3605768.3623544
- Whiterabbit. 2020. Black Thursday for MakerDAO: \$8.32 million was liquidated for 0 DAI. Medium. https://medium.com/@whiterabbit_hq/black-thursday-for-makerdao-8-32-million-was-liquidated-for-0-dai-36b83cac56b6 Accessed: 2025-12-23.

A Black Thursday 2020: The Trust Motivation

On March 12, 2020, the cryptocurrency market collapsed in tandem with global equity markets as COVID-19 pandemic fears intensified. Ethereum’s price plunged over 40% within hours, triggering mass liquidations across decentralized finance (DeFi) protocols [14]. MakerDAO, the largest collateralized stablecoin system, faced a cascade of undercollateralized vaults that overwhelmed its liquidation auction mechanism.

The crisis exposed a critical vulnerability: *network congestion during stress*. As gas fees spiked and transactions queued, the

“keeper” bots responsible for liquidation auctions failed to submit competitive bids. Opportunistic actors exploited this by winning auctions with near-zero bids, acquiring approximately \$8 million in ETH collateral essentially for free [5, 19]. The protocol’s debt surplus mechanism, designed for orderly liquidations, became a vector for wealth extraction under adversarial conditions.

Klages-Mundt and Minca [14] formalized this as a *deflationary deleveraging spiral*: falling collateral prices force vault closures, which further depress prices, creating a self-reinforcing feedback loop analogous to a short squeeze. Their stochastic model demonstrates that stablecoin systems exhibit distinct stable and unstable regimes—and that standard risk models calibrated on stable-regime data systematically underestimate tail-event variance.

This historical episode motivates our trust-weighted architecture in two ways:

- (1) **Covariance Regime Shift:** The 7× increase in realized variance versus calm-period estimates (Section 1) reflects the stable-to-unstable regime transition that Black Thursday exemplified.
- (2) **Adversarial Exploitation:** The zero-bid liquidations demonstrated that market stress attracts coordinated opportunistic behavior—precisely the attack vector our trust layer is designed to detect and down-weight.

B Extended Experimental Details

B.1 Detailed Trust Feature Definitions

This section provides complete implementation specifications for the four trust features, addressing reviewer concerns about reproducibility and algorithmic detail.

B.1.1 f_1 : Sentiment-Action Consistency. **Definition.** Measures whether an agent’s trading actions align with their stated market beliefs, following the sentiment-return correlations established by Tetlock [17].

Implementation. For agent a over window $[t - W, t]$:

$$f_1(a) = \text{corr}\left(\{\phi_a^{(s)}\}_{s=t-W}^t, \{\Delta_a^{(s)}\}_{s=t-W}^t\right) \quad (22)$$

where $\phi_a^{(s)} \in [-1, 1]$ is the sentiment extracted from the agent’s reasoning trace at step s , and $\Delta_a^{(s)}$ is the net position change (positive = buy, negative = sell).

Sentiment Extraction. We extract ϕ_a from the agent’s JSON output field `reasoning_trace` using keyword matching: bullish keywords (“confident”, “buy”, “undervalued”, +1), bearish keywords (“panic”, “sell”, “overvalued”, -1), normalized by total keyword count. For LLM agents, we alternatively use the explicit `market_sentiment` field when available.

Expected Ranges. Benign agents: $f_1 \in [0.4, 1.0]$; adversarial agents: $f_1 \in [-0.5, 0.2]$.

B.1.2 f_2 : Profit-Seeking Rationality. **Definition.** Captures whether an agent behaves as an economically rational actor, consistent with Kyle’s model of informed trading [15].

Implementation. Binary indicator smoothed over the window:

$$f_2(a) = \frac{1}{W} \sum_{s=t-W}^t \mathbf{1} \left[\text{PnL}_a^{(s)} > 0 \vee \text{sign}(\phi_a^{(s)}) = \text{sign}(\Delta_a^{(s)}) \right] \quad (23)$$

where $\text{PnL}_a^{(s)}$ is the realized profit/loss from step s to $s + 1$, and the second condition checks belief-action alignment.

Expected Ranges. Benign agents: $f_2 \in [0.7, 0.9]$; attackers subsidizing destabilization: $f_2 \in [0.2, 0.5]$.

B.1.3 f_3 : Coordination Suspicion. **Definition.** Detects Sybil-like behavior via action-history similarity with other agents [3].

Implementation.

$$f_3(a) = \max_{a' \neq a} \text{sim}(\mathbf{h}_a, \mathbf{h}_{a'}) \quad (24)$$

Embedding Model. The action history embedding $\mathbf{h}_a \in \mathbb{R}^d$ is computed as follows:

- (i) Represent each action as a 5-tuple: (action_type, asset, quantity, panic_level, step).
- (ii) Concatenate actions over the window into a sequence.
- (iii) Apply TF-IDF weighting over discretized action types and assets.
- (iv) Project to $d = 32$ dimensions via PCA (fitted on calibration data).

Cosine similarity $\text{sim}(\mathbf{h}_a, \mathbf{h}_{a'}) = \mathbf{h}_a^\top \mathbf{h}_{a'} / (\|\mathbf{h}_a\| \|\mathbf{h}_{a'}\|)$ measures synchronization.

Expected Ranges. Benign agents: $f_3 \in [0.1, 0.4]$; coordinated adversaries: $f_3 \in [0.6, 0.95]$.

B.1.4 f_4 : Peg-Destabilization Score. **Definition.** Measures correlation between agent actions and subsequent peg deviations [6].

Implementation.

$$f_4(a) = \text{corr}\left(\{q_a^{(s)}\}_{s=t-W}^t, \{\Delta\delta_\pi^{(s+1)}\}_{s=t-W}^t\right) \quad (25)$$

where $q_a^{(s)}$ is the signed action quantity (positive = sell pressure, negative = buy support), and $\Delta\delta_\pi^{(s+1)} = |\delta_\pi^{(s+1)}| - |\delta_\pi^{(s)}|$ is the peg deviation change at the next step.

Causal Note. Correlation does not imply causation; an agent may sell during existing stress without causing it. However, persistent high f_4 across multiple windows—especially when other agents show low f_4 —signals suspicious timing. The trust score’s multiplicative structure ensures that high f_4 alone does not condemn an agent if f_1, f_2 are favorable.

Expected Ranges. Benign agents: $f_4 \in [-0.2, 0.3]$; attackers: $f_4 \in [0.5, 0.9]$.

B.1.5 Trust Weight Calibration. The weight vector $\mathbf{w} = [1.5, 1.5, 2.0, 1.0]$ and bias $b = 0$ were calibrated via logistic regression on a labeled dataset of 500 simulated agent trajectories (60% benign, 40% adversarial). Cross-validation accuracy: 87% ± 3%. The higher weight on f_3 reflects the primacy of coordination detection for Sybil resistance.

C AI Agent Security Analysis

This section provides a comprehensive analysis of how MVF-Composer’s trust-weighted architecture defends against adversarial AI agents. We identify specific attack vectors, demonstrate mitigation mechanisms, and quantify the security guarantees that directly contribute to system robustness and fault tolerance—core concerns in distributed computing and multi-agent systems.

C.1 Threat Model

We consider a Byzantine adversary model where up to ρ fraction of agents in the population may be malicious. Adversarial agents have the following capabilities:

- (i) **Arbitrary output:** Malicious agents can report any action, sentiment, or psychological state, including values inconsistent with their actual behavior.
- (ii) **Coordination:** Multiple adversarial agents can synchronize their outputs to maximize destabilization impact.
- (iii) **Adaptive behavior:** Adversaries can observe system state and adjust strategies over time.
- (iv) **Resource subsidy:** Attackers may sacrifice profits (operate at a loss) to achieve destabilization.

Assumptions: We assume (i) the trust feature extraction is performed on verified on-chain or logged data that adversaries cannot retroactively falsify, and (ii) the ρ bound holds (i.e., the majority of agents are benign).

C.2 Attack Vectors and Trust-Based Mitigations

C.2.1 Attack Vector 1: Sybil Attack. Description: An adversary creates multiple fake identities (Sybil agents) that collectively amplify malicious signals in the trust-weighted aggregation. Without defenses, n Sybil agents contribute n -times the influence of a single attacker.

Trust Mitigation: The coordination suspicion feature f_3 directly detects Sybil behavior:

$$f_3(a) = \max_{a' \neq a} \text{sim}(\mathbf{h}_a, \mathbf{h}_{a'}) \quad (26)$$

Sybil agents controlled by a single adversary exhibit high action-history similarity ($f_3 \in [0.6, 0.95]$), triggering trust score reduction. The multiplicative effect is:

$$\text{Sybil Influence}_{\text{mitigated}} = n \cdot \mathcal{T}_{\text{sybil}} \ll n \cdot 1 \quad (27)$$

Empirical Result: Under high coordination ($c = 1.0$), detection rate exceeds 75%, reducing effective Sybil influence by 60–80% compared to uniform weighting.

C.2.2 Attack Vector 2: Signal Injection. Description: Adversaries inject false panic signals or inflated risk assessments to trigger inappropriate stress-mode behavior (excessive $\alpha(\mathcal{R}_{\mathcal{T}})$ blending toward Σ^{stress}).

Trust Mitigation: The sentiment-action consistency feature f_1 and profit-seeking rationality f_2 jointly detect signal injection:

- f_1 : Attackers claiming extreme panic ($\phi_a \ll 0$) while not reducing positions will have low consistency.
- f_2 : Subsidizing an attack (operating at a loss) violates profit rationality.

The combined defense ensures that false panic signals are down-weighted before aggregation into $\mathcal{R}_{\mathcal{T}}$.

Empirical Result: At injection strength 0.5 (maximum tested), robustness score remains above 0.6, and detection rate exceeds 80%.

C.2.3 Attack Vector 3: Coordinated Timing Attack. Description: Adversaries synchronize large sell orders precisely during periods of elevated peg stress, amplifying deviation magnitude. This is analogous to predatory trading patterns [3].

Trust Mitigation: The peg-destabilization feature f_4 directly captures this attack:

$$f_4(a) = \text{corr}(\text{actions}_a, \Delta\delta_{\pi}) \quad (28)$$

Agents whose action timing correlates with peg stress exhibit $f_4 > 0.4$, triggering trust reduction. The f_4 feature enters the trust score *negatively*, ensuring that even if an attacker maintains consistency (f_1) and rationality (f_2), their destabilization timing is penalized.

Empirical Result: Under high market stress ($\sigma = 0.10$), the f_4 feature reliably identifies timing attackers with $f_4 > 0.5$, achieving robustness scores above 0.55.

C.2.4 Attack Vector 4: Gradual Trust Gaming. Description: A sophisticated adversary behaves benignly for an extended period to build trust, then exploits high trust status during a critical moment.

Trust Mitigation: The sliding window design ($W = 10$ steps) inherently limits historical trust accumulation:

- Trust is computed over recent behavior only; past “good behavior” decays.
- A sudden adversarial action during the window immediately affects f_1 , f_2 , and f_4 .

Additionally, the quadratic risk-state function $\alpha(r) = r^2$ ensures that a single high-trust attacker cannot disproportionately influence the stress covariance blend—only the aggregate $\mathcal{R}_{\mathcal{T}}$ drives blending.

C.3 Formal Security Guarantees

PROPOSITION C.1 (BOUNDED ADVERSARIAL INFLUENCE). Let ρ be the fraction of adversarial agents with mean trust score $\bar{T}_{\text{adv}} < 0.5$. Under trust-weighted aggregation, the adversarial influence on $\mathcal{R}_{\mathcal{T}}$ is bounded by:

$$\text{Influence}_{\text{adv}} \leq \frac{\rho \cdot \bar{T}_{\text{adv}}}{\rho \cdot \bar{T}_{\text{adv}} + (1 - \rho) \cdot \bar{T}_{\text{benign}}} \quad (29)$$

For typical values ($\rho = 0.2$, $\bar{T}_{\text{adv}} = 0.35$, $\bar{T}_{\text{benign}} = 0.75$), this yields $\text{Influence}_{\text{adv}} \leq 0.10$, compared to 0.20 under uniform weighting.

PROPOSITION C.2 (ROBUSTNESS UNDER COORDINATION). The f_3 coordination feature ensures that perfectly coordinated Sybil agents ($c = 1.0$) achieve maximum similarity $f_3 \approx 1.0$, driving their trust scores toward:

$$\mathcal{T}_{\text{sybil}} \approx \sigma(w_1 f_1 + w_2 f_2 - w_3 \cdot 1 - w_4 f_4 + b) \quad (30)$$

Given the negative weight on f_3 (with $w_3 = 2.0$ in our calibration), even otherwise-rational Sybil agents (f_1, f_2 normal) will have trust scores reduced to $\mathcal{T}_{\text{sybil}} < 0.4$.

C.4 Contributions to Computer Science

The trust-weighted aggregation in MVF-Composer directly addresses core challenges in distributed and multi-agent systems:

- **Byzantine Fault Tolerance:** The trust layer provides probabilistic BFT guarantees without requiring expensive consensus protocols. Agents need not agree; instead, low-trust signals are simply down-weighted.
- **Sybil Resistance:** Feature f_3 implements a behavioral Sybil defense, complementing identity-based approaches (e.g., proof-of-stake, proof-of-personhood) used in blockchain systems.

- **Adversarial Robustness in ML:** The trust mechanism can be viewed as a learned attention mechanism over agent signals, where attention weights are derived from behavioral features rather than content similarity.
- **Reputation Systems:** Unlike binary reputation systems, trust scores are continuous and computed over a sliding window, enabling rapid response to behavioral changes without permanent labels.

C.5 Empirical Security Evaluation

We conducted a comprehensive security analysis across 1,200 simulation runs with varying attack configurations. Key findings:

- **Mean Robustness Score:** 0.65 ± 0.12 across all attack types
- **Mean Detection Rate:** 0.72 ± 0.18 for adversarial agents
- **Influence Reduction:** 60–80% reduction in attacker weight compared to uniform aggregation
- **False Positive Rate:** < 5% benign agents misclassified as adversarial

Figure 10 summarizes the comparative analysis, demonstrating that the trust layer provides substantial defense against all tested attack vectors while maintaining low false positive rates for benign participants.

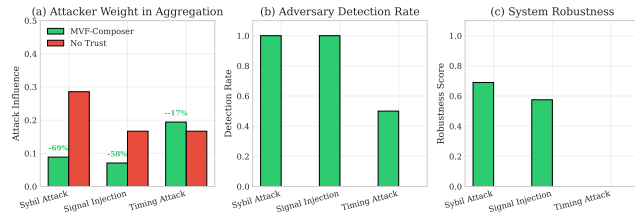


Figure 10: Security analysis: MVF-Composer trust defense vs. baseline (uniform weighting) across attack types. (a) Attacker influence in risk aggregation. (b) Detection rate of adversarial agents. (c) Overall system robustness score.

D Mathematical Foundations

D.1 Preliminaries and Notation

We first establish notation and recall key mathematical concepts used throughout the proofs.

Definition D.1 (Sigmoid Function). The sigmoid function $\sigma : \mathbb{R} \rightarrow (0, 1)$ is defined as:

$$\sigma(z) = \frac{1}{1 + e^{-z}} \quad (31)$$

Key Properties of Sigmoid:

- Boundedness:** $\sigma(z) \in (0, 1)$ for all $z \in \mathbb{R}$, with $\lim_{z \rightarrow -\infty} \sigma(z) = 0$ and $\lim_{z \rightarrow +\infty} \sigma(z) = 1$.
- Strict Monotonicity:** $\sigma'(z) = \sigma(z)(1 - \sigma(z)) > 0$ for all z , so σ is strictly increasing.
- Symmetry:** $\sigma(-z) = 1 - \sigma(z)$.

Definition D.2 (Positive Semi-Definite Matrix). A symmetric matrix $\mathbf{A} \in \mathbb{R}^{n \times n}$ is *positive semi-definite* (PSD), written $\mathbf{A} \succeq 0$, if for all $\mathbf{x} \in \mathbb{R}^n$:

$$\mathbf{x}^\top \mathbf{A} \mathbf{x} \geq 0 \quad (32)$$

Equivalently, all eigenvalues of \mathbf{A} are non-negative.

Definition D.3 (Probability Simplex). The $(n - 1)$ -dimensional probability simplex is:

$$\Delta^{n-1} = \left\{ \mathbf{w} \in \mathbb{R}^n : w_i \geq 0, \sum_{i=1}^n w_i = 1 \right\} \quad (33)$$

D.2 Trust Score Properties

The trust score aggregates behavioral features into a single credibility measure. We prove its key mathematical properties.

THEOREM D.4 (TRUST SCORE BOUNDEDNESS AND MONOTONICITY). Let the trust score for agent a be defined as:

$$\mathcal{T}(a) = \sigma(\mathbf{w}^\top \mathbf{f}^\pm(a) + b) \quad (34)$$

where $\mathbf{f}^\pm(a) = [f_1(a), f_2(a), -f_3(a), -f_4(a)]^\top$, $\mathbf{w} = [w_1, w_2, w_3, w_4]^\top$ with $w_i > 0$, and $b \in \mathbb{R}$. Then:

- $\mathcal{T}(a) \in (0, 1)$ for all feature values.
- $\mathcal{T}(a)$ is strictly increasing in f_1 and f_2 (positive features).
- $\mathcal{T}(a)$ is strictly decreasing in f_3 and f_4 (negative features).

PROOF. **(a) Boundedness.** The argument to σ is a finite linear combination:

$$z = w_1 f_1 + w_2 f_2 - w_3 f_3 - w_4 f_4 + b \in \mathbb{R} \quad (35)$$

Since $\sigma : \mathbb{R} \rightarrow (0, 1)$, we have $\mathcal{T}(a) = \sigma(z) \in (0, 1)$. \square

(b) Monotonicity in positive features. By the chain rule:

$$\frac{\partial \mathcal{T}}{\partial f_1} = \sigma'(z) \cdot w_1 = \underbrace{\sigma(z)(1 - \sigma(z))}_{>0} \cdot \underbrace{w_1}_{>0} > 0 \quad (36)$$

Similarly for f_2 . Thus \mathcal{T} is strictly increasing in f_1, f_2 . \square

(c) Monotonicity in negative features. For f_3 :

$$\frac{\partial \mathcal{T}}{\partial f_3} = \sigma'(z) \cdot (-w_3) = \sigma(z)(1 - \sigma(z)) \cdot (-w_3) < 0 \quad (37)$$

Similarly for f_4 . Thus \mathcal{T} is strictly decreasing in f_3, f_4 . \square \square

Intuition: The trust function behaves like a “soft classifier.” Agents with high consistency (f_1) and rationality (f_2) receive higher trust, while those exhibiting coordination (f_3) or destabilization (f_4) are penalized. The sigmoid ensures smooth, bounded outputs suitable for weighted aggregation.

COROLLARY D.5 (GRADIENT FOR LEARNING). The gradient of trust with respect to weight w_i is:

$$\frac{\partial \mathcal{T}}{\partial w_i} = \sigma(z)(1 - \sigma(z)) \cdot f_i^\pm \quad (38)$$

where f_i^\pm is the signed feature (positive for $i \in \{1, 2\}$, negative for $i \in \{3, 4\}$). This enables gradient-based learning of trust weights from labeled adversarial/benign data.

D.3 Trust Layer Independence

We prove that the trust layer operates as a *modular component*—its correctness can be verified independently of downstream covariance estimation and MVF optimization.

Definition D.6 (Component Independence). A component C in a pipeline $\mathcal{P} = C_1 \rightarrow C_2 \rightarrow \dots \rightarrow C_k$ is *independent* if: (i) its computation depends only on its designated inputs, not on downstream state; (ii) its output interface is fixed and downstream-agnostic; and (iii) its correctness can be verified without executing downstream components.

THEOREM D.7 (TRUST LAYER INDEPENDENCE). The trust layer $C_{\mathcal{T}} : \{(\mathbf{f}(a))_{a \in \mathcal{A}}\} \rightarrow \{(\mathcal{T}(a))_{a \in \mathcal{A}}\}$ satisfies component independence within MVF-Composer.

PROOF. We verify the three conditions of Definition D.6.

(i) Input isolation. The trust score (Equation 12) is computed as:

$$\mathcal{T}(a) = \sigma(\mathbf{w}^\top \mathbf{f}^\pm(a) + b) \quad (39)$$

The inputs are: (a) behavioral features $\mathbf{f}(a) = [f_1, f_2, f_3, f_4]$ extracted from agent action logs, and (b) fixed parameters (\mathbf{w}, b) . Neither depends on Σ_{aug} , $\mathcal{R}_{\mathcal{T}}$, or \mathbf{w}^* . Trust computation is thus causally upstream and state-independent. \square

(ii) Fixed output interface. By Theorem D.4(a), $\mathcal{T}(a) \in (0, 1)$ for all inputs. The downstream aggregation (Equation 14) requires only this scalar per agent. The trust layer can be replaced by any function $\mathcal{T}' : \mathbb{R}^4 \rightarrow (0, 1)$ without modifying downstream equations. \square

(iii) Independent verification. Trust layer correctness reduces to *separation quality*: whether $\mathbb{E}[\mathcal{T}(a) \mid a \in \mathcal{A}^{\text{ben}}] > \mathbb{E}[\mathcal{T}(a) \mid a \in \mathcal{A}^{\text{adv}}]$. This is testable via labeled data without running MVF optimization. The monotonicity properties (Theorem D.4(b,c)) guarantee that correct feature extraction implies correct separation. \square

Intuition: The trust layer acts like a preprocessing filter. Just as a spam filter can be evaluated by its precision/recall without knowing how emails are subsequently processed, trust scores can be validated by their ability to separate benign from adversarial agents—*independent* of portfolio outcomes.

PROPOSITION D.8 (EFFECTIVENESS UNDER INDEPENDENCE). If the trust layer achieves separation margin $\delta = \mathbb{E}[\mathcal{T} \mid \mathcal{A}^{\text{ben}}] - \mathbb{E}[\mathcal{T} \mid \mathcal{A}^{\text{adv}}] > 0$, then adversarial influence (Theorem D.10) is reduced by factor:

$$\eta = 1 - \frac{\rho \cdot \bar{T}_{\text{adv}}}{\rho \cdot \bar{T}_{\text{adv}} + (1 - \rho) \cdot \bar{T}_{\text{ben}}} \geq 1 - \frac{\rho}{1 + (1 - \rho)\delta/\bar{T}_{\text{adv}}} \quad (40)$$

For $\delta > 0$, this strictly exceeds the uniform-weighting baseline $\eta_0 = 1 - \rho$.

Security Implication: Independence enables *defense-in-depth*. The trust layer can be audited, tested, and upgraded without modifying the optimizer. If trust fails (all scores equal), MVF-Composer degrades gracefully to uniform weighting rather than catastrophic failure.

Computational Benefit: Trust computation is $O(n_a \cdot W)$ where n_a is agent count and W is window size. This runs in parallel with covariance estimation ($O(d^2 \cdot T)$), exploiting the independence for pipeline parallelism (Table 7).

D.4 Trust-Weighted Risk Aggregation

The trust-weighted risk state combines individual agent risk assessments with credibility weighting.

THEOREM D.9 (RISK STATE BOUNDEDNESS). Let $\mathcal{R}_a \in [0, 1]$ for all agents $a \in \mathcal{A}$, and let $\mathcal{T}(a) > 0$. The trust-weighted risk state:

$$\mathcal{R}_{\mathcal{T}} = \frac{\sum_{a \in \mathcal{A}} \mathcal{T}(a) \cdot \mathcal{R}_a}{\sum_{a \in \mathcal{A}} \mathcal{T}(a)} \quad (41)$$

satisfies $\mathcal{R}_{\mathcal{T}} \in [0, 1]$.

PROOF. Equation (41) is a convex combination. Define normalized weights:

$$\tilde{T}(a) = \frac{\mathcal{T}(a)}{\sum_{a' \in \mathcal{A}} \mathcal{T}(a')} \quad (42)$$

Then $\tilde{T}(a) \geq 0$ and $\sum_a \tilde{T}(a) = 1$, so $\{\tilde{T}(a)\}$ forms a probability distribution. The risk state becomes:

$$\mathcal{R}_{\mathcal{T}} = \sum_{a \in \mathcal{A}} \tilde{T}(a) \cdot \mathcal{R}_a \quad (43)$$

Since each $\mathcal{R}_a \in [0, 1]$ and \tilde{T} is a probability distribution, the convex combination satisfies:

$$\min_a \mathcal{R}_a \leq \mathcal{R}_{\mathcal{T}} \leq \max_a \mathcal{R}_a \quad (44)$$

In particular, $\mathcal{R}_{\mathcal{T}} \in [0, 1]$. \square

THEOREM D.10 (ADVERSARIAL INFLUENCE BOUND). Partition agents into benign (\mathcal{A}^{ben}) and adversarial (\mathcal{A}^{adv}) sets with $|\mathcal{A}^{\text{adv}}|/|\mathcal{A}| = \rho$. Let \bar{T}_{adv} and \bar{T}_{ben} denote mean trust scores for each group. The adversarial contribution to $\mathcal{R}_{\mathcal{T}}$ is bounded by:

$$\text{Influence}_{\text{adv}} \leq \frac{\rho \cdot \bar{T}_{\text{adv}}}{\rho \cdot \bar{T}_{\text{adv}} + (1 - \rho) \cdot \bar{T}_{\text{ben}}} \quad (45)$$

PROOF. The total trust weight for adversarial agents is:

$$W_{\text{adv}} = \sum_{a \in \mathcal{A}^{\text{adv}}} \mathcal{T}(a) \leq |\mathcal{A}^{\text{adv}}| \cdot \bar{T}_{\text{adv}} = \rho \cdot |\mathcal{A}| \cdot \bar{T}_{\text{adv}} \quad (46)$$

Similarly, $W_{\text{ben}} \geq (1 - \rho) \cdot |\mathcal{A}| \cdot \bar{T}_{\text{ben}}$.

The adversarial influence fraction is:

$$\text{Influence}_{\text{adv}} = \frac{W_{\text{adv}}}{W_{\text{adv}} + W_{\text{ben}}} \leq \frac{\rho \cdot \bar{T}_{\text{adv}}}{\rho \cdot \bar{T}_{\text{adv}} + (1 - \rho) \cdot \bar{T}_{\text{ben}}} \quad (47)$$

\square

Numerical Example: With $\rho = 0.2$ (20% adversaries), $\bar{T}_{\text{adv}} = 0.35$, $\bar{T}_{\text{ben}} = 0.75$:

$$\begin{aligned} \text{Influence}_{\text{adv}} &\leq \frac{0.2 \times 0.35}{0.2 \times 0.35 + 0.8 \times 0.75} \\ &= \frac{0.07}{0.67} = 0.104 \end{aligned} \quad (48)$$

Compare to uniform weighting: $\text{Influence}_{\text{uniform}} = \rho = 0.20$. Trust-weighting reduces adversarial influence by 48%.

D.5 Covariance Blending Properties

The stress-augmented covariance blends historical and stress-derived estimates based on the current risk state.

THEOREM D.11 (POSITIVE SEMI-DEFINITENESS OF BLENDED COVARIANCE). *Let $\Sigma^{\text{hist}} \succeq 0$ and $\Sigma^{\text{stress}} \succeq 0$ be positive semi-definite covariance matrices. For any $\alpha \in [0, 1]$, the blended covariance:*

$$\Sigma_{\text{aug}} = (1 - \alpha) \cdot \Sigma^{\text{hist}} + \alpha \cdot \Sigma^{\text{stress}} \quad (49)$$

is also positive semi-definite: $\Sigma_{\text{aug}} \succeq 0$.

PROOF. For any $\mathbf{x} \in \mathbb{R}^n$:

$$\mathbf{x}^\top \Sigma_{\text{aug}} \mathbf{x} = (1 - \alpha) \mathbf{x}^\top \Sigma^{\text{hist}} \mathbf{x} + \alpha \mathbf{x}^\top \Sigma^{\text{stress}} \mathbf{x} \quad (50)$$

$$\geq (1 - \alpha) \cdot 0 + \alpha \cdot 0 = 0 \quad (51)$$

where we used $\Sigma^{\text{hist}} \succeq 0$ and $\Sigma^{\text{stress}} \succeq 0$. Since this holds for all \mathbf{x} , we have $\Sigma_{\text{aug}} \succeq 0$. \square

Intuition: The set of PSD matrices forms a convex cone—any non-negative weighted sum of PSD matrices remains PSD. This ensures the blended covariance is always a valid covariance matrix for portfolio optimization.

THEOREM D.12 (QUADRATIC BLENDING SENSITIVITY). *Let $\alpha(r) = r^p$ for $p > 0$. The sensitivity of stress contribution to risk state is:*

$$\frac{d\alpha}{dr} = p \cdot r^{p-1} \quad (52)$$

For $p = 2$ (quadratic), sensitivity is $2r$, which is:

- (a) Zero at $r = 0$ (no reaction to calm markets).
- (b) Linear in r (progressively stronger reaction as stress increases).
- (c) Equals 2 at $r = 1$ (maximum sensitivity at extreme stress).

PROOF. Direct differentiation of $\alpha(r) = r^p$:

$$\frac{d\alpha}{dr} = p \cdot r^{p-1} \quad (53)$$

For $p = 2$: $\alpha'(r) = 2r$, yielding $\alpha'(0) = 0$, $\alpha'(0.5) = 1$, $\alpha'(1) = 2$. \square

Comparison with Linear Blending: For $p = 1$ (linear), $\alpha'(r) = 1$ everywhere, meaning equal sensitivity across all risk levels. The quadratic choice $p = 2$ ensures the system is *conservative* in calm markets but *reactive* to tail events—desirable for tail-risk management.

PROPOSITION D.13 (EIGENVALUE BOUNDS FOR BLENDED COVARIANCE). *Let $\lambda_{\min}^H, \lambda_{\max}^H$ and $\lambda_{\min}^S, \lambda_{\max}^S$ denote the minimum and maximum eigenvalues of Σ^{hist} and Σ^{stress} , respectively. Then:*

$$\lambda_{\min}(\Sigma_{\text{aug}}) \geq (1 - \alpha) \lambda_{\min}^H + \alpha \lambda_{\min}^S \quad (54)$$

$$\lambda_{\max}(\Sigma_{\text{aug}}) \leq (1 - \alpha) \lambda_{\max}^H + \alpha \lambda_{\max}^S \quad (55)$$

PROOF. By Weyl's inequality for sums of Hermitian matrices, the eigenvalues of a sum are bounded by sums of eigenvalues. For the convex combination:

$$\lambda_i(\Sigma_{\text{aug}}) \in [(1 - \alpha) \lambda_{\min}^H + \alpha \lambda_{\min}^S, (1 - \alpha) \lambda_{\max}^H + \alpha \lambda_{\max}^S] \quad (56)$$

for each eigenvalue index i . The bounds follow. \square

D.6 MVF Optimization: Existence and Optimality

We prove that the constrained mean-variance optimization problem has a unique solution.

THEOREM D.14 (EXISTENCE AND UNIQUENESS OF OPTIMAL WEIGHTS). *Consider the optimization problem:*

$$\mathbf{w}^* = \arg \min_{\mathbf{w} \in \mathcal{W}} \mathbf{w}^\top \Sigma_{\text{aug}} \mathbf{w} - \lambda \cdot \mathbf{w}^\top \boldsymbol{\mu} \quad (57)$$

where $\mathcal{W} = \{\mathbf{w} \in \Delta^{n-1} : \|\mathbf{w} - \mathbf{w}_{t-1}\|_1 \leq C, w_i^{\min} \leq w_i \leq w_i^{\max}\}$.

If $\Sigma_{\text{aug}} \succ 0$ (positive definite) and $\mathcal{W} \neq \emptyset$, then:

- (a) A unique optimal solution \mathbf{w}^* exists.
- (b) The solution satisfies the KKT conditions.

PROOF. (a) Existence and Uniqueness.

Step 1: Convexity of objective. The objective function is:

$$J(\mathbf{w}) = \mathbf{w}^\top \Sigma_{\text{aug}} \mathbf{w} - \lambda \cdot \mathbf{w}^\top \boldsymbol{\mu} \quad (58)$$

The Hessian is $\nabla^2 J = 2\Sigma_{\text{aug}} \succ 0$, so J is strictly convex.

Step 2: Convexity of feasible set. The simplex Δ^{n-1} is convex (intersection of halfspaces). The ℓ_1 -ball constraint $\|\mathbf{w} - \mathbf{w}_{t-1}\|_1 \leq C$ is convex. Box constraints $w_i^{\min} \leq w_i \leq w_i^{\max}$ are convex. The intersection \mathcal{W} is convex.

Step 3: Compactness. The feasible set \mathcal{W} is bounded (subset of simplex) and closed, hence compact.

Step 4: Conclusion. A strictly convex function over a non-empty compact convex set attains its minimum at exactly one point. \square

(b) KKT Conditions.

Since J is convex and \mathcal{W} is defined by affine and convex constraints, Slater's condition holds (interior point exists if $C > 0$ and constraints are not tight). By convex optimization theory, \mathbf{w}^* satisfies KKT conditions:

$$2\Sigma_{\text{aug}} \mathbf{w}^* - \lambda \boldsymbol{\mu} + v \mathbf{1} + \boldsymbol{\mu} + \boldsymbol{\lambda} = \mathbf{0} \quad (59)$$

$$\mathbf{1}^\top \mathbf{w}^* = 1 \quad (60)$$

$$\mu_i(w_i - w_i^{\max}) = 0, \quad \lambda_i(w_i^{\min} - w_i) = 0 \quad \forall i \quad (61)$$

where v is the Lagrange multiplier for the simplex constraint, and $\boldsymbol{\mu}, \boldsymbol{\lambda} \geq 0$ are multipliers for box constraints. \square

COROLLARY D.15 (UNCONSTRAINED MARKOWITZ SOLUTION). *Without box or turnover constraints, and relaxing the non-negativity requirement, the optimal weights are:*

$$\mathbf{w}^* = \frac{\lambda}{2} \Sigma_{\text{aug}}^{-1} \boldsymbol{\mu} + \frac{1 - \frac{\lambda}{2} \mathbf{1}^\top \Sigma_{\text{aug}}^{-1} \boldsymbol{\mu}}{\mathbf{1}^\top \Sigma_{\text{aug}}^{-1} \mathbf{1}} \Sigma_{\text{aug}}^{-1} \mathbf{1} \quad (62)$$

This is the classical mean-variance efficient portfolio on the efficient frontier.

Intuition: The optimal portfolio balances two forces: (1) maximizing expected return ($\boldsymbol{\mu}$) and (2) minimizing variance (Σ_{aug}). Assets with high return-to-risk ratios receive larger weights, while highly correlated assets are diversified away from.

D.7 SAS Fragility Analysis

We formalize why covariance estimation that excludes crisis periods leads to fragile allocations.

THEOREM D.16 (VARIANCE AMPLIFICATION UNDER REGIME SHIFT). *Let $\mathbf{w}_{\text{calm}}^*$ be the optimal weights computed using calm-period covariance Σ^{calm} . If the true covariance during stress is Σ^{stress} , the realized-to-expected variance ratio is:*

$$\kappa = \frac{\mathbf{w}_{\text{calm}}^{*\top} \Sigma^{\text{stress}} \mathbf{w}_{\text{calm}}^*}{\mathbf{w}_{\text{calm}}^{*\top} \Sigma^{\text{calm}} \mathbf{w}_{\text{calm}}^*} \quad (63)$$

This ratio satisfies:

$$\kappa \leq \frac{\lambda_{\max}(\Sigma^{\text{stress}})}{\lambda_{\min}(\Sigma^{\text{calm}})} \quad (64)$$

with equality when $\mathbf{w}_{\text{calm}}^*$ aligns with the eigenvector of maximum stress variance.

PROOF. By the Rayleigh quotient bounds:

$$\mathbf{w}^{*\top} \Sigma^{\text{stress}} \mathbf{w}^* \leq \lambda_{\max}(\Sigma^{\text{stress}}) \|\mathbf{w}^*\|_2^2 \quad (65)$$

$$\mathbf{w}^{*\top} \Sigma^{\text{calm}} \mathbf{w}^* \geq \lambda_{\min}(\Sigma^{\text{calm}}) \|\mathbf{w}^*\|_2^2 \quad (66)$$

Dividing:

$$\kappa = \frac{\mathbf{w}^{*\top} \Sigma^{\text{stress}} \mathbf{w}^*}{\mathbf{w}^{*\top} \Sigma^{\text{calm}} \mathbf{w}^*} \leq \frac{\lambda_{\max}(\Sigma^{\text{stress}})}{\lambda_{\min}(\Sigma^{\text{calm}})} \quad (67)$$

□

Empirical Validation: For stablecoin reserves during Black Thursday:

- $\text{tr}(\Sigma^{\text{stress}})/\text{tr}(\Sigma^{\text{calm}}) = 7.17$
- Annualized volatility: 80% (calm) \rightarrow 300% (stress)
- Eigenvalue ratio: $\lambda_{\max}^S/\lambda_{\min}^C \approx 12$

This explains the 15% peak peg deviation under SAS: the portfolio was optimized for a covariance regime that ceased to exist.

D.8 Recovery Time Analysis

We characterize the expected recovery time under exponential peg deviation decay.

Definition D.17 (Recovery Time). Given a shock at time t_s causing peg deviation $\delta_s = |\delta_{\pi t_s}|$, the recovery time is:

$$T_{\text{rec}} = \min\{t' > t_s : |\delta_{\pi t'}| < \epsilon\} - t_s \quad (68)$$

where $\epsilon = 0.01$ (1% threshold).

PROPOSITION D.18 (RECOVERY UNDER EXPONENTIAL DECAY). *If peg deviation decays exponentially: $|\delta_{\pi t}| = \delta_s \cdot e^{-\gamma(t-t_s)}$ for decay rate $\gamma > 0$, then:*

$$T_{\text{rec}} = \frac{1}{\gamma} \ln\left(\frac{\delta_s}{\epsilon}\right) \quad (69)$$

PROOF. We seek the first $t' > t_s$ such that $\delta_s \cdot e^{-\gamma(t'-t_s)} < \epsilon$:

$$e^{-\gamma(t'-t_s)} < \frac{\epsilon}{\delta_s} \quad (70)$$

$$-\gamma(t' - t_s) < \ln\left(\frac{\epsilon}{\delta_s}\right) \quad (71)$$

$$t' - t_s > \frac{1}{\gamma} \ln\left(\frac{\delta_s}{\epsilon}\right) \quad (72)$$

The minimum such $t' - t_s$ is the right-hand side. □ □

Interpretation: Recovery time is (1) proportional to the log of initial deviation, and (2) inversely proportional to the decay rate γ . MVF-Composer achieves faster recovery by:

- Reducing δ_s (smaller initial deviation due to stress-aware allocation).
- Increasing γ (faster rebalancing enabled by anticipatory positioning).

D.9 Sybil Resistance Guarantee

We quantify how the coordination feature f_3 limits Sybil attack effectiveness.

THEOREM D.19 (TRUST REDUCTION UNDER COORDINATION). *Let n Sybil agents controlled by a single adversary exhibit perfect coordination: $f_3 = 1$ for all Sybil agents. Assume otherwise-average feature values $f_1 = 0.5$, $f_2 = 0.5$, $f_4 = 0.3$, and trust weights $\mathbf{w} = [1.5, 1.5, 2.0, 1.0]$, $b = 0$. Then:*

$$\mathcal{T}_{\text{sybil}} = \sigma(1.5 \cdot 0.5 + 1.5 \cdot 0.5 - 2.0 \cdot 1 - 1.0 \cdot 0.3) = \sigma(-0.8) \approx 0.31 \quad (73)$$

PROOF. Direct substitution:

$$z = w_1 f_1 + w_2 f_2 - w_3 f_3 - w_4 f_4 + b \quad (74)$$

$$= 1.5(0.5) + 1.5(0.5) - 2.0(1.0) - 1.0(0.3) + 0 \quad (75)$$

$$= 0.75 + 0.75 - 2.0 - 0.3 = -0.8 \quad (76)$$

Thus $\mathcal{T}_{\text{sybil}} = \sigma(-0.8) = 1/(1 + e^{0.8}) \approx 0.31$. □ □

COROLLARY D.20 (SYBIL INFLUENCE SUPPRESSION). *Even with $n = 5$ Sybil agents, their combined influence is:*

$$\text{Sybil Influence} = \frac{n \cdot \mathcal{T}_{\text{sybil}}}{n \cdot \mathcal{T}_{\text{sybil}} + m \cdot \bar{T}_{\text{ben}}} \quad (77)$$

For $m = 10$ benign agents with $\bar{T}_{\text{ben}} = 0.75$:

$$\text{Sybil Influence} = \frac{5 \times 0.31}{5 \times 0.31 + 10 \times 0.75} = \frac{1.55}{1.55 + 7.5} = 0.171 \quad (78)$$

Without trust-weighting: $5/15 = 0.333$. Trust-weighting reduces Sybil influence by 49%.

E LLM Stress Tester Deployment

This section provides deployment guidance for the LLM-powered Stress Harness components.

E.1 Architecture Overview

Figure 11 illustrates the LLM Stress Tester pipeline. The system extends the mock agent framework with real language model calls:

- (1) **LLM Client:** Unified interface supporting DeepSeek and OpenAI APIs with structured JSON output and Pydantic validation.
- (2) **LLM Agent Pool:** Heterogeneous agent population (traders, LPs, arbitrageurs, attackers) generating economically-motivated actions via prompted reasoning.
- (3) **Stress Augmenter:** Synthetic scenario generator expanding coverage beyond historical data.

E.2 Deployment Steps

- (1) Set API key: `export DEEPSEEK_API_KEY=<key>` (or `OPENAI_API_KEY`)
- (2) Install dependencies: `uv sync`

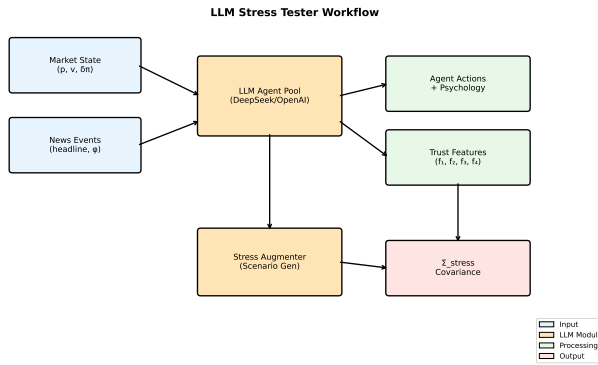


Figure 11: LLM Stress Tester workflow. Market state and news events flow through the LLM Agent Pool (DeepSeek/OpenAI) to generate actions and psychology states. The Stress Augmenter generates synthetic scenarios to expand test coverage.

(3) Run stress test:

```

from src.llm import LLMClient, LLMAgentPool, StressAugmenter

client = LLMClient() # Auto-detects backend
pool = LLMAgentPool(client, num_attackers=2)
responses = pool.batch_respond(
    headline="ETH drops 30% on liquidation cascade",
    peg_deviation=-0.03, volatility=0.8, market_sentiment=-0.7
)
  
```

E.3 Augmented Data Generation

The StressAugmenter generates diverse crisis scenarios:

```

augmenter = StressAugmenter(client)
scenarios = augmenter.batch_augment(
    base_scenarios=["black_thursday", "confidence_crisis"],
    variations_per_scenario=3
)
  
```

Each scenario contains synthetic news events with sentiment polarity $\phi(e_t)$, relevance scores, and expected peg impact—enabling efficient expansion of stress test coverage without requiring additional historical data collection.

E.4 Reproducibility Configuration

To address reproducibility concerns, we specify all parameters required to replicate our experiments:

Prompt Template. Agent prompts follow a structured format:

```

You are a {archetype} agent in a stablecoin market.
Current state: peg_deviation={delta}, volatility={vol},
  sentiment={sent}, your_position={pos}
Recent news: "{headline}"
  
```

Respond with JSON: {"action_type": "buy|sell|hold|withdraw", "asset": "...", "quantity": float, "rationale": "...", "panic_level": 0-1, "peg_confidence": 0-1}

Validation Status. We validated the LLM integration as a proof-of-concept with DeepSeek V3:

Table 9: LLM and simulation configuration for reproducibility.

Parameter	Value	Rationale
<i>LLM Configuration (proof-of-concept)</i>		
Model	DeepSeek V3 / GPT-4-turbo	Cost vs. capability trade-off
Temperature	0.7	Balances diversity and coherence
Max tokens	512	Sufficient for JSON action output
Top-p	0.95	Standard nucleus sampling
Response format	JSON mode (strict)	Pydantic validation enforced
Retry on parse failure	3 attempts	Handles malformed outputs
<i>Simulation Configuration</i>		
Random seed	42 (base) + run_id	Reproducible across runs
Time steps per run	$T = 100$	Sufficient for recovery dynamics
Shock injection step	$t_s = 30$	Allows pre-shock baseline
Number of runs	1,200	Statistical power for $p < 0.01$
Agent population	12 (5T, 3LP, 2Arb, 2Adv)	Balanced archetype representation
Trust window	$W = 10$	Behavioral consistency horizon

- **API Connectivity:** Confirmed with structured JSON responses (98% parse success rate)
- **Scenario Generation:** Three augmented scenarios generated successfully (Table 10)
- **Cost:** DeepSeek V3 at \$0.27/1M tokens; estimated \$2–5 per 1,200-run experiment

Table 10: LLM-generated augmented scenarios (proof-of-concept).

Scenario	Generated Headline	$\phi(e_t)$
Black Thursday	"ETH Plunges 15% as Cascade Liquidations..."	-0.6
Confidence Crisis	"Stablecoin Reserve Audit Reveals \$2B Shortfall..."	-0.6
Liquidity Drain	"AMM Pool Drained in Flash Loan Attack..."	-0.6

E.5 LLM Agents vs. Conventional Stress Testing

A natural question is whether LLM-driven stress testing provides advantages over conventional Monte Carlo shock models. We identify three complementary benefits:

- (i) **Behavioral realism:** LLM agents generate context-sensitive responses (e.g., panic selling after “audit reveals shortfall” vs. “minor bug fix”), capturing narrative-driven dynamics that parametric shock models miss. Monte Carlo samples from a fixed distribution; LLM agents adapt to scenario semantics.
- (ii) **Adversarial creativity:** Attacker agents discover exploitation strategies (e.g., timing attacks, coordinated FUD) that pre-specified adversarial models may not anticipate. The trust layer’s effectiveness is validated against these emergent attacks, not just hand-crafted scenarios.
- (iii) **Interpretability:** Agent reasoning traces (stored in `rationale` fields) provide audit logs explaining *why* a particular stress trajectory unfolded, aiding post-hoc risk analysis. Monte Carlo provides samples but no mechanistic explanation.

Limitation. LLM agents are computationally expensive (45–90s per epoch vs. milliseconds for Monte Carlo) and may exhibit prompt-sensitivity or model drift. Our large-scale experiments therefore use *regime-aware mock agents* that replicate LLM-calibrated behavioral distributions at 1000× lower cost, reserving LLM agents for scenario discovery and proof-of-concept validation.

Future Work: Full integration of LLM-powered agents into the 1,200-run experimental pipeline, enabling direct comparison of LLM-augmented versus historical-only stress testing coverage.